A Rapid Method for Modeling Transient River Response Under Stochastic Controls With Applications to Sea Level Rise and Sediment Nourishment

Arkesteijn, Liselot; Blom, Astrid; Labeur, Robert Jan

DOI
10.1029/2021JF006177

Publication date
2021

Document Version
Final published version

Published in
Journal of Geophysical Research: Earth Surface

Citation (APA)
Arkesteijn, L., Blom, A., & Labeur, R. J. (2021). A Rapid Method for Modeling Transient River Response Under Stochastic Controls With Applications to Sea Level Rise and Sediment Nourishment. *Journal of Geophysical Research: Earth Surface*, *126*(12), Article e2021JF006177. https://doi.org/10.1029/2021JF006177

JGR Earth Surface

RESEARCH ARTICLE
10.1029/2021JF006177

A Rapid Method for Modeling Transient River Response Under Stochastic Controls With Applications to Sea Level Rise and Sediment Nourishment

Liselot Arkesteijn[1], Astrid Blom[1], and Robert Jan Labeur[1]

[1]Faculty of Civil Engineering and Geosciences, Delft University of Technology, Delft, The Netherlands

Key Points:

- We propose a method to rapidly model river response under stochastic controls of flow rate, sediment discharge, and downstream water level
- The proposed method provides a computationally cheap alternative to the mean outcome of Monte Carlo analysis
- Sea level rise initially induces bed erosion where enhanced backwater effects or spatial changes of channel width reduce the sediment flux

Correspondence to:
A. Blom,
astrid.blom@tudelft.nl

Citation:
Arkesteijn, L., Blom, A., & Labeur, R. J. (2021). A rapid method for modeling transient river response under stochastic controls with applications to sea level rise and sediment nourishment. *Journal of Geophysical Research: Earth Surface*, *126*, e2021JF006177. https://doi.org/10.1029/2021JF006177

Received 23 MAR 2021
Accepted 23 NOV 2021

Abstract Recent analysis of equilibrium and quasi-equilibrium channel geometry in engineered (fixed-width) rivers has successfully shown that two temporal scales can be distinguished, with quasi-static (long-term) and dynamic (short-term) components. This distinction is based on the fact that channel slope cannot keep pace with short-term fluctuations of the controls. Here we exploit the distinction between the two temporal scales to model the transient (so time-dependent) phase of channel response, which is the phase wherein the channel approaches its new equilibrium. We show that: (a) besides channel slope, also the bed surface texture cannot keep pace with short-term fluctuations of the controls, and (b) mean transient channel response is determined by the probability distributions of the controls (e.g., flow duration curve rather than flow rate sequence). These findings allow us to set up a rapid numerical method that determines the mean transient channel response under stochastic controls. The method is based on distinguishing modes (i.e., sets of controls) and takes the probability density of each mode into account. At each time step, we compute the mode-specific flow, sediment transport rate, and corresponding change in bed level and surface texture. The net change within the time step is computed by weighting the mode-specific changes in bed level and surface texture with the probability density of each mode. The resulting mean transient channel response is a deterministic one, despite the controls being stochastic variables. We show that the proposed method provides a rapid alternative to Monte Carlo analysis regarding the mean time-dependent channel response.

Plain Language Summary Recent analysis of equilibrium and quasi-equilibrium channel geometry in engineered (fixed-width) rivers has successfully shown that two temporal scales can be distinguished, with quasi-static (long-term) and dynamic (short-term) components. This distinction allowed for a rapid model of a river's equilibrium state, and here we use the same distinction of time scales to set up a rapid numerical method that determines the mean transient channel response under stochastic controls. The method is based on distinguishing modes for the sets of controls, and accounts for the probability density of each mode. We show that the proposed method provides a rapid alternative to Monte Carlo analysis regarding the mean time-dependent channel response.

1. Introduction

When addressing channel response to natural or anthropogenic change of the controls, one needs to distinguish between three channel response phases: the initial, transient, and equilibrium phase (Blom, Arkesteijn, et al., 2017). The initial phase usually only lasts several days or weeks and is here defined as the phase wherein only the flow has time to adjust to the new situation. Adjustment of the river morphodynamic state cannot take place within the initial phase due to its short duration and the typically much longer time scale of morphodynamic adjustment. The equilibrium phase is the stage in which, by definition, the channel has reached the equilibrium or graded state associated with the new specifications of the controls. The transient phase of channel response marks the period in between: it covers the phase of adjustment (with associated downstream or upstream migrating adjustment waves) of channel slope, channel width, and bed surface texture after the initial phase has been completed and before the equilibrium phase has started. The transient phase may last several years, decades, or even centuries. Although not considered in this analysis, the initial phase can be accompanied by sudden morphodynamic change such as a flood-induced avulsion.

The time scales of morphodynamic channel response reflect how fast a reach responds in the transient phase regarding adjustment of channel slope, channel width, and bed surface texture to changes in the controls of equilibrium channel geometry (Blom, Chavarrías, et al., 2017; De Vries, 1975; Howard, 1982). These controls

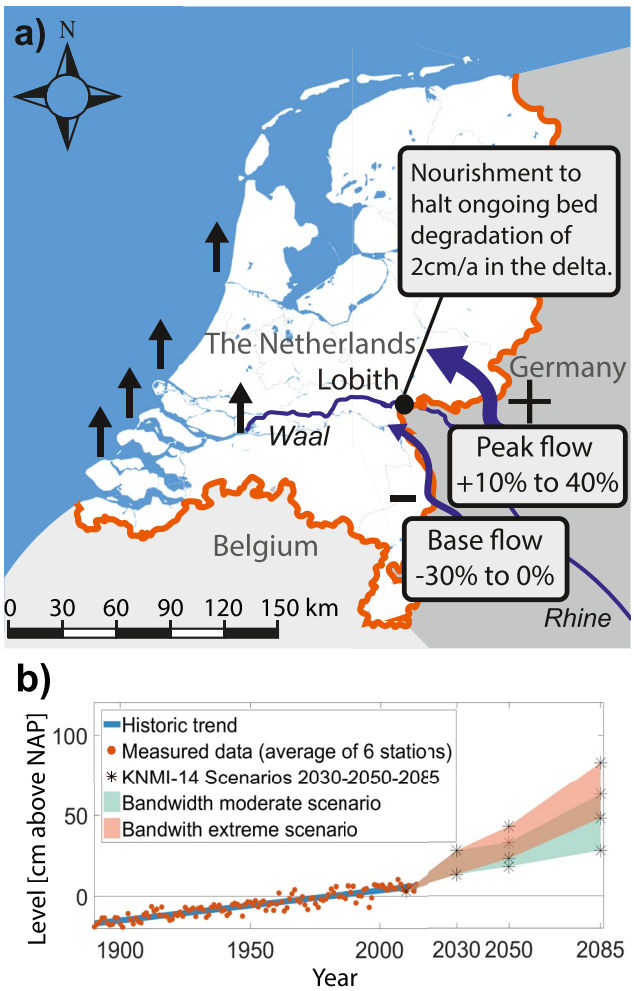

Figure 1. (a) Specifications of the controls for the Dutch Rhine in 2085, and (b) relative sea level with respect to NAP, a vertical datum used in large parts of Western Europe (Klein Tank et al., 2015).

include the hydrograph, the grainsize-specific sediment fluxes (i.e., the part of the sediment flux that is bed-material load), and base level (Mackin, 1948; Lane, 1957; Blom et al., 2016; Blom, Arkesteijn, et al., 2017). The time scale of channel response typically is large (De Vries, 1975), which implies that short-term fluctuations of the controls are not reflected in the channel response and that the flow duration curve (i.e., the range of flow rates and their probability density) rather than the time-varying hydrograph determines the channel response (Arkesteijn et al., 2019; Howard, 1982; Viparelli et al., 2012).

The change of controls may be gradual, for example, a slowly increasing sea level at the river mouth. When the controls change slowly compared to the time scale of channel response, channel geometry can keep pace with the changing controls (i.e., a quasi-equilibrium state, Blom, Chavarrías, et al., 2017; Howard, 1982). Under such conditions, channel geometry is characterized by the equilibrium state corresponding to the prevailing controls at all times.

Alternatively, changes in the controls can appear relatively sudden, which is typically the case when changes in the controls result from engineering works. River training (for instance dams, groynes or training dams) increases flood safety, navigability or benefits other river functions, and locally affects the controls and thereby induce morphodynamic changes in the river system (Van Vuren et al., 2015). The river response to these interventions is also characterized by the three phases of river response. The time scale of the transient response depends on the extent of the intervention and characteristics of the river system wherein the intervention takes place: for example, in the Dutch Rhine the time scale of transient response to domain-wide narrowing due to groynes may be several hundreds of years and of the order of years regarding local floodplain widening (De Vriend, 2015; De Vries, 1975).

The fact that channel slope is typically unaffected by short-term changes of the controls allows for the "static slope approximation," which was originally proposed for equilibrium and quasi-equilibrium conditions by Arkesteijn et al. (2019), under unisize sediment conditions. In the current analysis we extend the static slope approximation to the transient phase of channel response as well as to mixed-size sediment conditions. In other words, the static slope approximation is here extended to the "static slope-texture approximation." Although bed slope and surface texture are assumed to be quasi-static over the short timescale of control changes, they do adjust over the time scale of transient channel response.

As such, we hypothesize that the distinction between the two time scales of changes in the controls (i.e., short-term and long-term changes) and the associated static slope approximation are not only fundamental to channel equilibrium and quasi-equilibrium (Arkesteijn et al., 2019), but also to transient channel response. Our first objective is to illustrate that the mean component of transient channel response (i.e., averaged over the results associated with the stochastic controls) is governed by the joint probability density function of the controls and is not affected by the sequence of the values for these controls. This enables us to formulate a rapid statistics-based method for describing the mean transient channel response, which comprises our second objective.

The proposed method is particularly suitable for scenario analysis. Climate change is expected to lead to higher peak flow rates in the Rhine River in winter, longer periods of drought in summer, and an expected sea level rise between 25 and 80 cm in 2085 (Klijn et al., 2015; Klein Tank et al., 2015), which is illustrated in Figure 1. River response to such changes is typically analyzed through defining scenarios for the changing probability distribution of the controls or boundary conditions.

Section 2 presents the new statistics-based method for describing the mean transient channel response. Section 3 lists the simplifying assumptions of our model and its numerical properties. We consider two test cases to

evaluate whether the proposed method provides a sound alternative to predicting mean transient channel response based on Monte Carlo analysis: Case 1 addresses transient channel response to sea level rise (Section 4) and Case 2 (Section 5) considers transient channel response to sediment nourishment or local addition of sediment, which is a measure often used to mitigate domain-wide channel bed erosion (Quick et al., 2020; Ylla Arbós et al., 2021). In the Dutch Rhine river, nourishments are carried out at Lobith to counteract an ongoing bed degradation of approximately 2 cm per year (Figure 1). The time scale of channel response in Case 2 is an engineering scale and much smaller than the timescale of Case 1. As such, Case 2 is expected to be more challenging regarding the applicability of the proposed method.

2. The Proposed Method (vs. the Traditional Monte Carlo Method)

The proposed method is based on the distinction between two time scales (short-term and long-term) of changes of the controls. Its foundation is the elementary assumption that slope and bed surface texture are not affected by short-term changes of the controls, as their response is associated with a longer time scale. This "static slope-texture approximation" allows us to assume that all flow rates can be represented simultaneously, by weighting with their probability of occurrence, instead of occurring sequentially as in a traditional hydrograph. Worded differently, we impose the full probability distribution of controls at each time step rather than a realization from that probability distribution.

The conventional approach for solving a hydro-morphodynamic model in large river systems is a decoupled one. The validity of the decoupled approach results from the fact that in lowland rivers hydrodynamic change typically proceeds much faster than morphodynamic change (e.g., De Vries, 1975). Consequently, flow and changes of bed level and surface texture do only weakly interact and therefore their interaction on a very short time scale may be neglected. This allows for solving the hydrodynamic and morphodynamic equations consecutively instead of simultaneously. It has been shown that such decoupling of the equations is acceptable for values of the Froude number smaller than 0.7 approximately (Chavarrías et al., 2019; De Vries, 1965; Lyn, 1987; Lyn & Altinakar, 2002), which is typically considered a valid approximation for lowland rivers.

We compare the flow chart of the proposed method (Figure 2b) with the one of a conventional morphodynamic model (Figure 2a) applied in a Monte Carlo setting (e.g., Huthoff et al., 2010; Van Vuren et al., 2016). The new method distinguishes sets of hydrodynamic controls (i.e., modes). Each mode is associated with a certain probability density that represents the likelihood for the set of hydrodynamic controls to occur. For each of these modes, a computation of mode-specific flow, (grainsize-specific) sediment transport rates, change of bed level, sediment fluxes from and to the active layer, and change of bed surface texture, is carried out. After that, we determine the net change of bed level and bed surface texture through weighting the mode-specific values with the mode-specific probability density.

Mass conservation of bed surface sediment in the traditional Monte Carlo method is described using the Exner (1920) equation for unisize sediment conditions and using the Hirano (1971) equations for mixed-size sediment (e.g., Blom & Parker, 2004; Paola & Voller, 2005). The Hirano (1971) active layer model is based on a homogeneous bed surface layer (i.e., the active layer), which represents the bed sediment that is being reworked by the flow.

Figure 3 shows a schematic representation of the main variables in the Hirano active layer model and in the proposed model. In both models, the active layer has a thickness L_a, which is typically associated with the dune height or grain size (e.g., Ribberink, 1987). Within the active layer, the grain size distribution of the bed sediment does not vary vertically, and in the substrate below, the grain size may vary with vertical position.

For solving the active layer model using a numerical method, the substrate is discretized by defining vertical cells below the active layer. Each substrate cell has a thickness $L_{s,j}$ and composition $f_{s,j}$. If the bed aggrades, the active layer shifts upward, and part of the sediment in the active layer is transferred to the top substrate layer. If the bed degrades, the opposite occurs and material from the substrate is transferred to the active layer. In addition, if the bed aggrades, bed load material may be directly deposited in the substrate (Hoey & Ferguson, 1994).

The proposed method uses the Exner (1920) equation in unisize sediment conditions, similar to the Monte Carlo model. For mixed-size sediment conditions, the proposed method adapts the Hirano (1971) model by introducing an additional bed layer between the active layer and the substrate. This "dynamic layer" accounts for the sediment

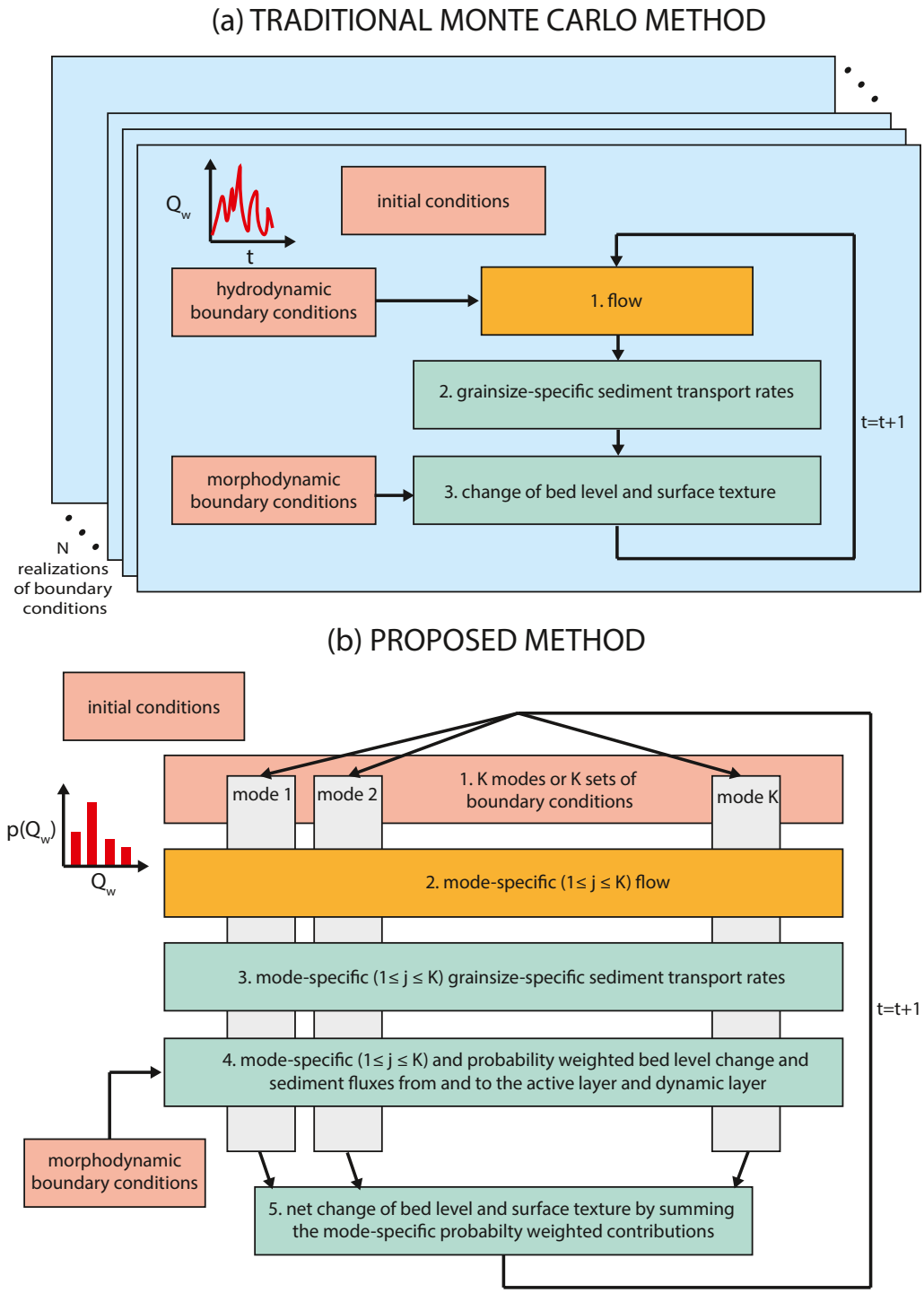

Figure 2. Flow chart of (a) the traditional Monte Carlo method where typically a large number (*N*) of runs is made with varying realizations of initial and/or boundary conditions, and (b) the proposed method for solving the mean component of transient channel response under stochastic controls.

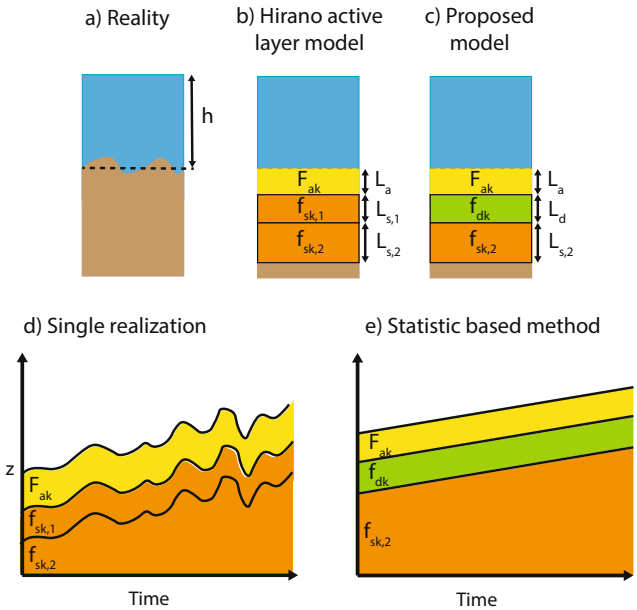

Figure 3. Schematic representation of (a) reality; (b) the traditional Hirano active layer model, and (c) the proposed method (i.e., the Hirano active layer model combined with a dynamic layer). Panels (d) and (e) show the development over time. A single realization of the Monte Carlo simulation based on the Hirano active layer model shows vertical fluctuations in bed level and associated vertical grain size fluxes. The dynamic layer compensates for the neglect of these vertical dynamics.

that is reworked as a result of short-term flow variations that induce alternating aggradation and degradation of the channel bed and associated vertical sediment mixing. The dynamic layer compensates for the neglect of these vertical sediment fluxes.

The (possibly) intuitive solution to account for the alternating bed aggradation and degradation and deeper reworking of the bed is to increase the active layer thickness. However, this cannot be a solution, as the sorting celerity depends on the active layer thickness (e.g., Ribberink, 1987). As mentioned above, the solution adopted here is to include a dynamic layer between the active layer and the substrate. The mode-specific bed level change and sediment fluxes from and to the active layer are computed using a conventional Hirano-based model and weighted with the mode-specific probability density. The equations related to the sediment fluxes from and to the dynamic layer are detailed in Appendix A.

The proposed method is a two-layer model for conservation of mixed-size bed sediment (Blom, 2008; Blom & Parker, 2004). The dynamic layer is analogous to the exchange layer used in the Ribberink two-layer model for conservation of mixed-size bed sediment (Blom, 2008; Blom & Parker, 2004; Ribberink, 1987). This exchange layer accounts for sediment reworking due to occasionally large dunes, whereas the dynamic layer of the proposed method accounts for sediment reworking due to short-term flow variations. Another important difference is that Ribberink (1987) uses a parametric formulation to define the magnitude of the sediment fluxes between the active layer and the exchange layer, whereas in our proposed dynamic layer, the magnitude of the fluxes naturally follows from the sediment mass conservation equations.

The proposed method resembles the Roelvink (2006) parallel online approach and the Wilmink (2015) MORMERGE approach, which are developed for coastal problems under unisize sediment conditions. The parallel online approach accounts for different hydraulic forcing occurring during one tidal cycle, and MORMERGE for variable wave fields. The underlying assumptions of both approaches are the same as for the proposed method: if the time interval in which all tidal respectively wave conditions (e.g., ebb, flood, spring tide, neap tide, and storms) occur is small compared to the time scale of system response, all hydraulic forcing can be considered at the same time and sequence effects can be neglected.

In our analysis, we compare the results of the proposed method to those of a traditional Monte Carlo analysis. The latter is based on the traditional three-step sequential solution of flow, grainsize-selective sediment transport rates, and bed level (and surface texture) change (e.g., Cao & Carling, 2002). When used for scenario analysis, a large number (N) of runs can be made under varying initial or boundary conditions (Figure 2a) using a Monte Carlo analysis. This traditional Monte Carlo method yields not only the mean transient channel response but also the associated range of variation around the mean trend or uncertainty range (e.g., Van Vuren, 2005).

3. Model Specifications

We use two numerical models: one based on the proposed method in Figure 2b and one based on the traditional backwater-Hirano model for the Monte Carlo method in Figure 2a. Appendix A details the equations of the two models. These models consider the simplest possible situation that describes the essential physics of the problem (e.g., Paola & Leeder, 2011). Simplifying assumptions are the following:

1. the channel has a single-branch with a rectangular cross-section and no floodplain;
2. the channel banks are non-erodible (e.g., an engineered fixed-planform channel);
3. there is no lateral inflow or outflow of water and sediment along the reach (i.e., there are neither tributaries nor bifurcations);
4. bed sediment porosity is constant;
5. bed friction coefficient is constant;

6. flow is subcritical;
7. we apply the backwater equation (e.g., Chow, 1959) to describe the flow, rather than the more generic Saint-Venant (1871) equations. This implies that the model is valid in lowland rivers where flood waves have become elongated and the flow rate varies slowly (e.g., Meirovich et al., 1998). This further implies that we assume the initial phase of channel response takes place immediately;
8. sediment is non-cohesive, and either of a unisize nature (i.e., well-sorted sand) or a mixed-size nature (i.e., a mixture of well-sorted gravel and sand);
9. all sediment is transported as bed-material load; and
10. particle abrasion is negligible.

These assumptions typically allow for appreciating a river's qualitative response to changes in the controls. Moreover, they enable us to fundamentally test the behavior of the proposed method in comparison to the traditional Monte Carlo analysis.

We address two cases: Case 1 and Case 2, which deal with, respectively, the transient channel response to sea level rise and sediment nourishment. The two cases differ with respect to the response time scale. The time scale of channel response to sea level rise is typically long (a few centuries, De Vries, 1975), whereas the time scale of channel response to a sediment nourishment is much shorter (several years).

Parameters in these model applications are as follows: the channel width B is 300 m (Figure 4a), porosity of bed sediment n is 0.4; sand size d_s is 1 mm; gravel size d_g equals 10 mm; and the non-dimensional bed friction coefficient c_f is 0.007. We apply the sediment transport relation of Ashida and Michiue (1971) and assume capacity-based transport, which implies that the sediment transport rate instantaneously adjusts to changes in the flow (e.g., Phillips & Sutherland, 1989). These values are considered roughly representative for the Rhine river at Lobith at the German-Dutch border (Blom, Arkesteijn, et al., 2017). The constant α associated with the Hoey and Ferguson (1994) sediment flux in Equation A11 in Appendix A is set equal to 0.5.

Figure 4 schematically illustrates the domain of Cases 1 and 2. In Case 1, the domain length L is 800 km. This length enables to study the transient phase of river response in the three typical river segments (Arkesteijn et al., 2019; Blom, Arkesteijn, et al., 2017). In summary, each river reach can be characterized as an upstream boundary segment (UBS, also called hydrograph boundary layer), backwater segment (BWS), or quasi-normal flow segment (QNFS). In a UBS, the temporal variation of the sediment supply rate differs from the temporal variation of the sediment transport capacity, despite their mean values being similar or equal (Arkesteijn et al., 2019). This temporal mismatch leads to downstream migrating waves (An, Cui, et al., 2017; An, Fu, et al., 2017; Parker, 2004; Parker et al., 2008; Wong & Parker, 2006). A UBS forms downstream of, for instance, a confluence, bifurcation, or a spatial change in channel width or bed friction. In a BWS, the flow depth at the downstream end of the reach (under subcritical flow conditions) differs from the normal flow depth. This leads to an alternation of M1 or M2 backwater curves depending on the flow rate (Arkesteijn et al., 2019; Blom, Arkesteijn, et al., 2017; Chow, 1959; Lamb et al., 2012; Lane, 1957; Nittrouer et al., 2011, 2012) and alternating channel bed aggradation and incision (Chatanantavet & Lamb, 2014; Ganti et al., 2016). A BWS forms upstream of, for instance, the river mouth, a confluence, bifurcation, or change in channel width or bed friction. In a QNFS, the flow depth varies with the flow rate, yet the flow remains quasi-normal or quasi-uniform for each value of the flow rate (Arkesteijn et al., 2019; Blom, Arkesteijn, et al., 2017). By definition, spatial gradients in the flow velocity are small to negligible and, consequently, little to no bed level change occurs. Quasi-normal flow segments are found over the reaches that remain: they form where no BWS and UBS are present.

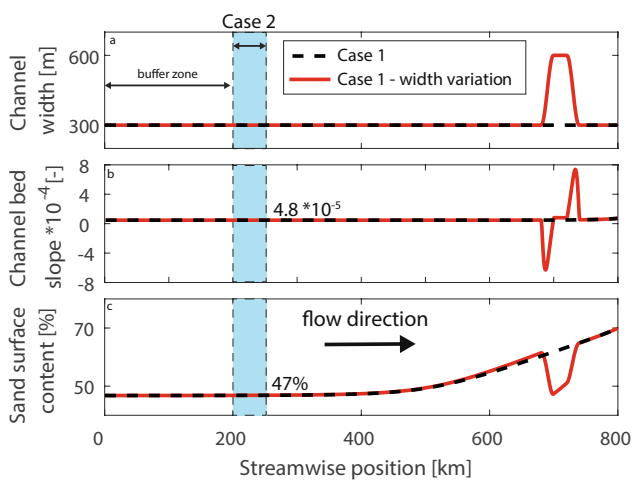

Figure 4. Channel width and initial conditions for all cases. Case 1a: constant width; and Case 1b: with spatial variations in channel width. The domain of Case 2 is also indicated.

The domain length of 800 km in Case 1 allows us to study river response in a BWS and QNFS. We include a 200 km buffer reach at the upstream end of the domain to remove fluctuations near the upstream boundary associated with the UBS. The buffer reach smoothens the fluctuations and ensures that at the river cross section at 200 km sediment transport enters our domain of interest at capacity. Our domain thus has a length of 600 km.

Besides Case 1a with a constant channel width of 300 m, we consider a Case 1b where the width is 600 m rather than 300 m over a 20 km long reach. As indicated in Figure 4a, it is characterized by a first portion where the channel width spatially increases, a second central portion where the channel width is 600 m, and a third portion where the channel width spatially decreases. Consequent to the spatial variation of channel width, UBSs are formed in the second central portion and in the channel downstream of the third portion, while BWSs are formed in the channel upstream and the second portion. The purpose of Case 1b is to analyze how the presence of UBSs affects the performance of the proposed method.

Case 2 has a domain length L of 50 km (see Figure 4). Sediment nourishment is modeled through imposing a 5 km long and instantaneous increase of bed level by 0.5 m (i.e., a hump), starting at 10 km downstream of the upstream end of the reach (i.e., at streamwise position 210 km). We set the grain size distribution of the nourished sediment equal to the one of the bed surface sediment in the initial (equilibrium) state. This case and its parameters are roughly based on the nourishment pilot at Lobith conducted in 2016 and 2019.

The dynamic layer thickness is determined by the depth of sediment reworking associated with short-term variations of the flow rate. Such sediment reworking is more relevant in UBSs and BWSs than in QNFSs. As a result, the dynamic layer thickness is typically smaller in QNFSs. The active layer thickness, L_a, is set equal to 1 m and the dynamic layer thickness, L_d, is 0.25 m for Case 1 and 0.1 m for Case 2. The dynamic layer thickness for Case 2 is smaller than Case 1, as Case 1 is governed by a BWS and Case 2 by a QNFS Appendix B further discusses the importance of the dynamic layer and illustrates the need for further research on the dynamic layer thickness.

In Case 1, we consider two scenarios for the rate of sea level rise: a mild sea level rise scenario, S1, of 3.5 mm/a and an extreme one, S2, of 10 mm/a. In Case 2, the downstream flow depth is set equal to the normal flow depth (i.e., it fluctuates with the varying water discharge), and is unaffected by backwater and sea level rise.

The hydrodynamic upstream boundary condition is the same in both cases, and is based on the hydrograph with discharges measured daily at Lobith (Bovenrijn) between the years 1901 and 2000 (Blom, Arkesteijn, et al., 2017). For the traditional Monte Carlo method, the hydrograph and corresponding sedigraph are subdivided in 100 series of a single year, which are ordered in various sequences to obtain $N = 100$ different hydrographs (i.e., 100 sequences of water discharge with equal flow duration curve). Each sequence of 100 years is repeated five times to construct a 500-year time series. Each of these time series provides the hydrodynamic upstream boundary condition for one of the N realizations.

For the proposed method, an empirical probability density function of water discharge is retrieved from the same hydrograph at Lobith, with discharges varying between a minimum discharge of 575 m^3/s and a maximum discharge of 13,000 m^3/s. In our two cases, the probability density function of water discharge is maintained constant (i.e., it does not evolve as a function of time, for instance, due to climate change).

The gravel and sand supply rates equal 0.11 and 0.56 Mt/a, respectively. The sedigraph agrees with the so-called "normal flow load distribution" (Blom, Arkesteijn, et al., 2017), which matches the (grainsize-specific) sediment transport rates under equilibrium conditions in a quasi-normal flow segment. For the proposed method the modes of the model are defined by a set of a water discharge value and a sediment discharge value that "would have occurred on the same time," accompanied by their probability of occurrence. Hence, for the proposed method the modes are defined based on the joint probability of the hydrograph and the corresponding sedigraph.

The downstream boundary condition is selected as a deterministic time series and, resultingly, is the same for all modes in Case 1, and depends on the water discharge and, resultingly, varies per mode in Case 2. We find that $K = 20$ is a sufficient number of sets of controls (i.e., modes). Appendix D provides more detailed information on the sensitivity of the results to the number of modes.

The initial condition of our runs is a dynamic equilibrium state regarding channel slope (or bed level) and bed surface texture (Arkesteijn et al., 2019; Blom et al., 2016; Blom, Arkesteijn, et al., 2017), which is shown in Figures 4b and 4c and computed using the model equations in Appendix C and the solution strategy discussed in Arkesteijn et al. (2019).

The initial channel slope S is constant within the QNFS (equal to $4.8 \cdot 10^{-5}$) and gradually steepens in the BWS toward the downstream end of the reach (Arkesteijn et al., 2019). This is because, with increasing streamwise position in a BWS, base flows become increasingly less effective in transporting the sediment flux downstream.

The channel slope increases with downstream position to compensate for this effect (Arkesteijn et al., 2019). Similarly, the sand surface content is uniform within the QNFS (sand surface content equals 47% in the active layer), and gradually increases with streamwise position within the BWS. This is because the difference in flow velocity between peak and base flow increases with streamwise position, and, as a result, the net mobility difference between fine and coarse sediment decreases with streamwise position. This streamwise decrease of the mobility difference is accompanied with streamwise decrease of the mean bed surface grain size. This is because, with a reduced mobility difference, the bed surface does not need to coarsen as much to provide sufficient mobility of the coarse sediment.

The initial grain size distribution of the dynamic layer sediment (proposed method) or the top substrate layer sediment (Monte Carlo runs) is finer than the active layer sediment. It is important to note that, in a dynamic equilibrium state, the top substrate is reworked by the flow as a result of alternating aggradation and erosion associated with short-term variations of the flow rate. This implies that the top part of the substrate has an equilibrium grain size distribution that is a weighted average of the active layer and annual bed load flux (associated with the Hoey and Ferguson approximation of the vertical sediment flux). The initial grain size distribution of the top substrate layer (or dynamic layer) is computed using Equation C13 in Appendix C. The initial grain size distribution of the (remaining) substrate is assumed to be uniform and set equal to the one of the annual sediment flux.

Both models have been implemented in the one-dimensional numerical research code Elv (e.g., Arkesteijn et al., 2019; Blom, Arkesteijn, et al., 2017; Chavarrías et al., 2019). We use a first order explicit Euler method to solve the backwater equation by stepping through space, and a first order explicit Euler method to solve the Hirano equation when stepping through time.

In Case 1 the spatial step, Δx, is 1,000 m. The time step, Δt, is half a month (i.e., 1/24 of a year) for the proposed method and 1 day for the traditional Monte Carlo method. The thickness of the top substrate layer, l_s, is 0.25 m in the Monte Carlo simulations. The same holds for the dynamic layer thickness for the proposed method. The thickness of each deeper substrate layer is 0.5 m. Hence both methods start from the same vertical stratification.

In Case 2, both methods use a spatial step, Δx, equal to 500 m. The time step Δt is 1 day for the proposed method and 4 hr for the traditional Monte Carlo method. The dynamic layer thickness and top substrate layer thickness equal 0.1 m, which also holds for the deeper substrate layers.

4. Case 1: Sea Level Rise

Case 1 considers transient channel response to sea level rise of a reach that initially is in a dynamic equilibrium state. The downstream base level increases linearly with time following either the mild S1 sea level rise scenario (3.5 mm/a) or the extreme S2 sea level rise scenario (10 mm/a).

Although the BWS, which roughly extends over the lower 350 km of the domain, shows a significant response to sea level rise within the first 100 years (Figures 5a and 5b), the channel response significantly lags behind the forcing. Within this period, the maximum rate of bed level rise is smaller than 1 mm/a (Figures 5c and 5d), whereas the downstream base level rises by respectively, 3.5 (S1) and 10 mm/a (S2).

Bed level rise lags behind the rate of sea level rise, but within the BWS, the rate of bed level rise does increase with time. This appears most clearly for the S2 scenario (Figures 5c and 5d). Sea level rise and the delayed response of the river bed imply that M1 backwater effects during base flows intensify with time, while the M2 backwater effects during peak flows reduce. As such, sediment is increasingly trapped within the BWS. The rate of bed level rise, however, does not increase until it is equal to the rate of sea level rise, as the sediment flux from upstream does not provide sufficient sediment for the bed to keep pace with rising sea level.

Equilibrium conditions still prevail in the QNFS positioned further upstream. Sea level rise leads to an upstream-migrating adjustment wave that extends the BWS in the upstream direction. The time scale of response to sea level rise typically is several hundreds of years (De Vries, 1975).

Temporal change in bed surface texture is small (Figures 5e and 5f). As the sand content in the sediment flux is much larger than the gravel flux, the intensified M1 backwaters during base flows within the BWS have the largest effect on sand mobility and lead to a mild preferential deposition of sand. As a result, the bed becomes slightly finer with time.

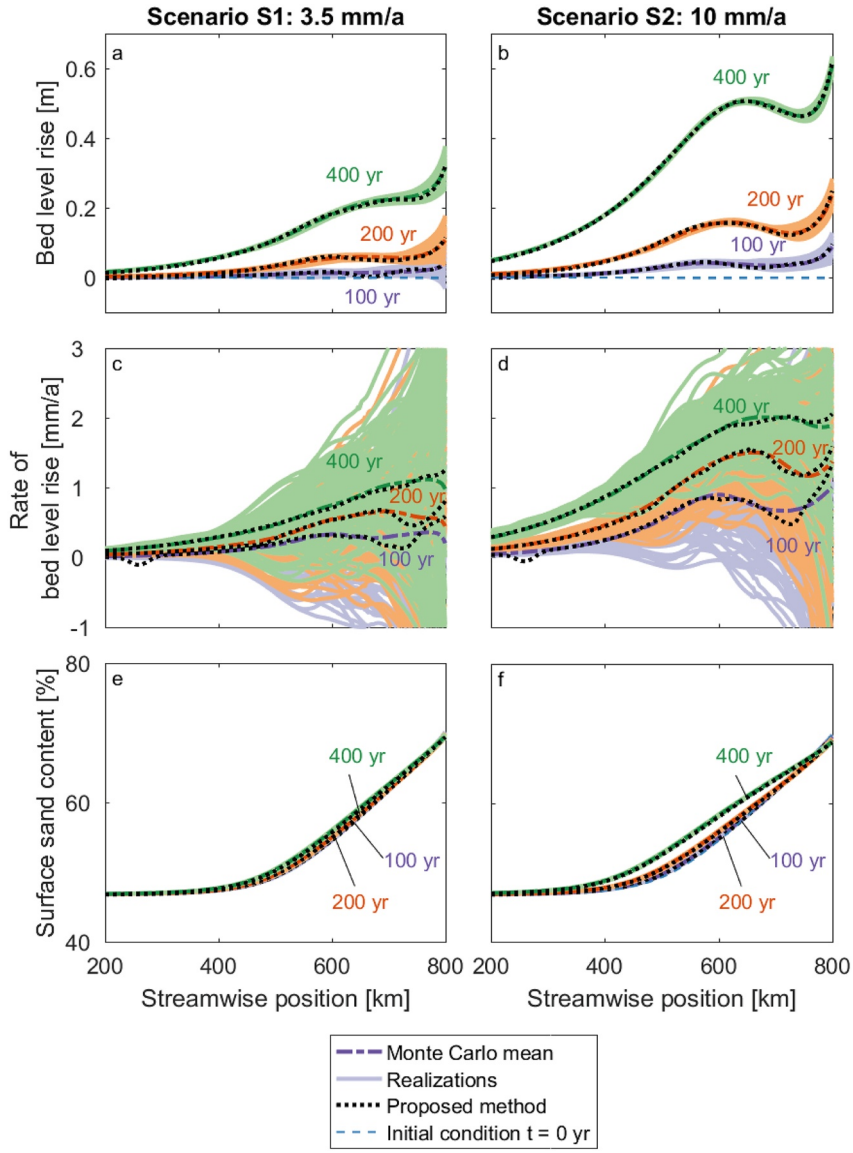

Figure 5. Transient channel response after 100, 200, and 400 years of a uniform-width channel (Case 1a) to the mild S1 sea level rise scenario (3.5 mm/a) and the extreme S2 sea level rise scenario (10 mm/a), according to the proposed method (black dotted line) versus the traditional Monte Carlo method (dash-dotted line). Panels (a) and (b) show bed level rise relative to the initial condition; panels (c) and (d) rates of bed level rise; and panels (e) and (f) the volume fraction content of sand in the bed surface sediment.

Importantly, Figure 5 shows that the differences between the proposed method and the traditional Monte Carlo method are negligible. This implies that for the chosen example the transient channel response to sea level rise depends on the flow duration curve only and not on the sequence of the flow rates, and confirms the applicability of the proposed method in this case.

Case 1b considers the response to sea level rise of a reach with a spatially varying channel width (channel width locally increases to 600 m, Figure 4) to study whether UBSs challenge the applicability of the proposed method. The reach is governed by two UBSs: the first one located directly downstream of the streamwise increase in channel width and the second one directly downstream of the streamwise decrease in channel width. At the locations along the channel reach where the width varies with streamwise position, the sediment transport capacity of the flow also varies with streamwise position. This may lead to alternating deposition and erosion, generating sediment waves to propagate through the channel sections downstream (Arkesteijn et al., 2019).

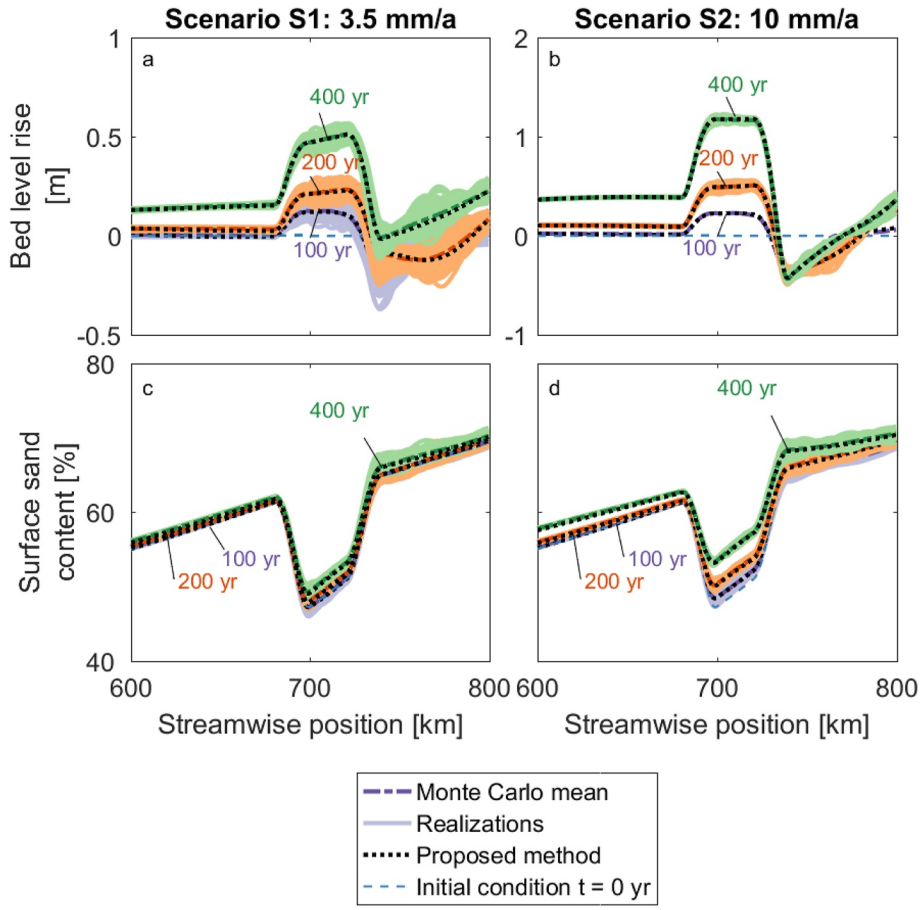

Figure 6. Transient channel response after 100, 200, and 400 years of a variable-width channel (Case 1b) to the mild S1 sea level rise scenario (3.5 mm/a) and the extreme S2 sea level rise scenario (10 mm/a), according to the proposed method (black dotted line) versus the traditional Monte Carlo method (dash-dotted line). Subplots a and b show bed level rise relative to the initial condition, and subplots c and d the volume fraction content of sand in the bed surface sediment. Please note the different vertical axes in panels (a) and (b).

The channel response to sea level rise comprises a superposition of two effects (Figures 6a and 6b): (i) a large-scale aggradational response to sea level rise, which is a trend similar to the one in Figure 5, and (ii) a wide-reach-related response, characterized by aggradation over the wide reach and erosion downstream of it.

This response to sea level rise is explained as follows. Sea level rise increases the flow depth over the BWS, that is, approximately the lower 350 km of the domain. As the flow depth in the wide reach is significantly smaller than elsewhere, its relative increase of flow depth due to sea level rise is larger than elsewhere, as well as the associated relative decrease of the sediment transport capacity. This results in deposition in the wide reach and, as a result, a decrease of the sediment supply to the downstream reach, which leads to channel bed incision downstream from the wide reach. This local and fast response is temporary: eventually the entire reach continues to aggrade according to the large-scale and slow response.

Importantly again, the result of the proposed method is very similar to the mean outcome of the traditional Monte Carlo method. This implies that the presence of the UBSs here does not limit the applicability of the proposed method.

Appendix D addresses the effect of the number of modes K for discretization of the probability density function of the controls. It shows that $K = 20$ modes is a sufficient number of modes to obtain accurate results.

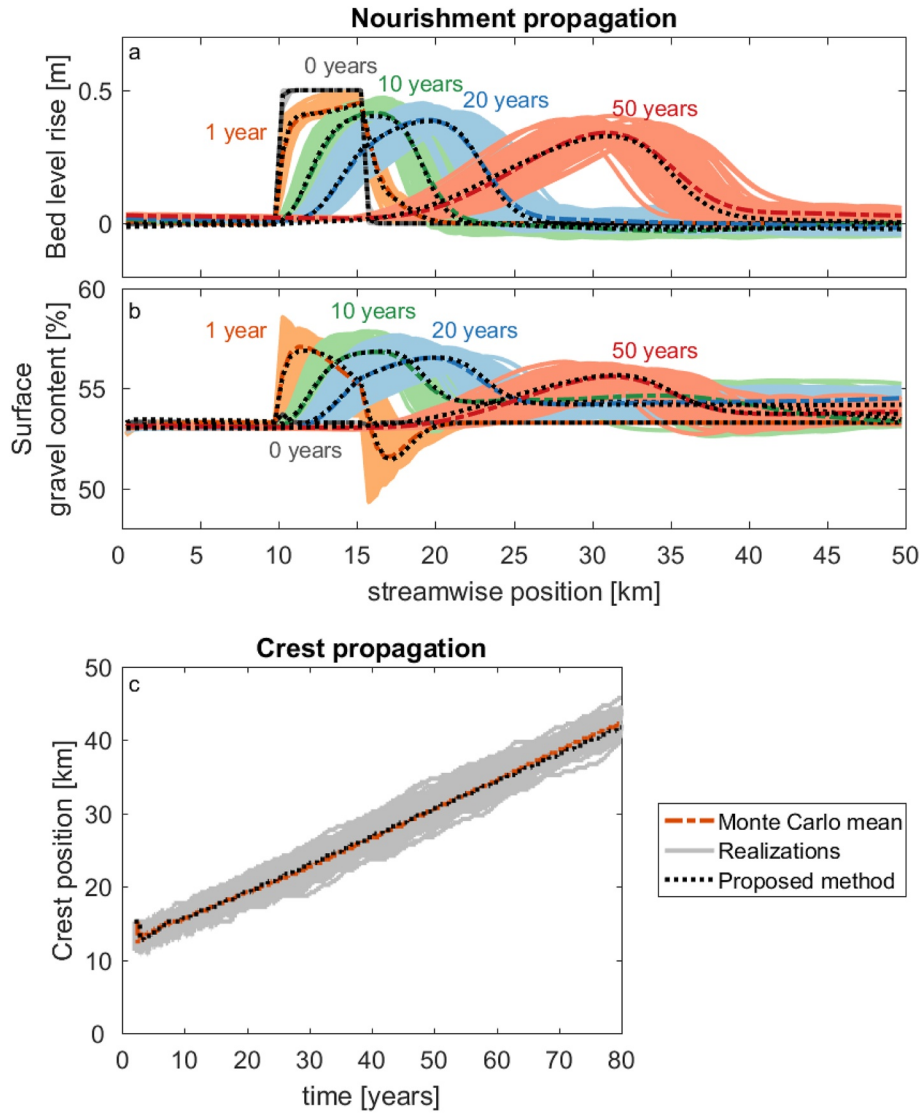

Figure 7. Transient channel response to sediment nourishment. Panels (a) and (b) show the change in bed level and bed surface texture, respectively. Panel (c) shows the time-space diagram of propagation of the crest.

5. Case 2: Sediment Nourishment

Case 2 addresses the translation and dispersion of nourished sediment in a uniform-width river reach to test the applicability of the proposed method to a channel response problem dominated by an engineering time scale. We consider sediment nourishment within a quasi-normal flow segment (Figure 4).

The sediment nourishment is introduced as a local instantaneous increase of the bed level. Such a locally elevated bed results in an M1 backwater upstream of the hump and an M2 drawdown curve over the elevated reach. The response at the start of the transient phase is governed by four effects (Figure 7):

1. The M1 backwater induces very mild sediment deposition and bed surface fining upstream of the hump.
2. At the upstream end of the hump, flow velocity abruptly increases with downstream position, which induces local erosion and bed surface coarsening at the upstream end of the elevated reach. This leads to a rapid coarsening of the elevated reach, starting from the upstream end of the hump and migrating downstream.
3. The M2 backwater over the elevated reach erodes the nourished sediment and enhances the coarsening of the bed surface over the elevated reach.

4. At the downstream end of the elevated reach, the vertical flow expansion reduces sediment mobility and sediment deposits (with preferential deposition of sand).

The flow expansion at the downstream end (Effect 4) results in deposition of gravel and sand. Together with the erosion at the upstream end of the hump (Effect 2), this leads to a slow propagation of the hump. Initially the deposited sediment consists of more sand than gravel, which temporarily fines the bed surface downstream of the elevated reach, the effect of which very rapidly migrates downstream. This temporary surface fining is because the flow expansion reduces the sand flux more strongly than the gravel flux, as the sand flux is larger than the gravel flux. As a result, the downstream-migrating coarse hump is preceded by a rapid downstream-migrating fining wave that goes together with a mild aggradational wave. Within the first 10 years, this wave moves through the 50 km long reach entirely and therefore it is only visible in Figure 7 after 1 year.

Figure 7 shows the change in bed level and surface texture resulting from the sediment nourishment at 0, 1, 10, 20, and 50 years after placement, as well as the streamwise displacement of the peak of the hump. The nourished sediment propagates downstream faster during high flow rates and slower during low flow rates, and the nourished sediment disperses while being transported downstream. The instantaneous propagation speed of the nourished sediment varies among the Monte Carlo realizations, but the mid-term average propagation speed for a single realization equals the mean or expected speed of all Monte Carlo realizations. Also, the mean propagation speed based on the traditional Monte Carlo method and the proposed method are approximately the same also on a shorter time scale (Figure 7c).

This result implies that for the considered case the flow duration curve governs the mean propagation of the nourished sediment and that the sequence of flow rates is unimportant, rendering the proposed method applicable for the prediction of the transient response to sediment nourishments.

6. Discussion

The presented cases have shown that the proposed method can successfully predict changes in bed level and bed texture over a period from several years to centuries. The method does not provide insight on the range of fluctuations around the mean transient channel response, which is output that a traditional Monte Carlo analysis does provide. Nevertheless, the fact that our method does not account for the short-term variations in the controls causing these fluctuations around the mean, has not limited its applicability. The proposed method may be used to study channel response in all segments (UBSs, QNFSs, and BWSs) of a lowland river, as demonstrated by the examples.

In our analysis, the stochastics of the controls have been limited to the stochastics of the flow rate. The upstream sediment flux was assumed to be dependent on the flow rate, and the flow depth at the downstream end was considered as a deterministic series (Case 1) or dependent on the flow rate (Case 2). Instead or additionally, the method may also include the stochastics of the downstream base level (tides and storms) (e.g., Bolla Pittaluga et al., 2015) or include a non-deterministic relation between flow discharge and sediment discharge. In these cases, the modes would be selected based on the joint probability density function of all boundary conditions. Further research would be required to see which number of modes K would be required to sufficiently cover the joint probability distribution.

As shown in our analysis, the (joint) probability density function can be assumed to be constant. Alternatively, and specifically suited in case of scenario studies, the probability density function of a control may be assumed to change over time. As an example, in the introduction it was explained that in the Dutch Rhine peak flows are expected to increase by 10%–40% in the coming years due to climate change, whereas the base flow rates would decrease up to 30%. The proposed method can incorporate such changes directly by gradually transforming the probabilities assigned to each discharge mode as a function of time.

The proposed method uses the static slope-texture approximation, which means that it assumes that channel slope and bed texture are typically unaffected by short-term changes of the controls. In terms of modeling assumptions, this limits the applicability of the proposed method to situations wherein (i) the hydrodynamic and morphodynamic solution may be decoupled (or solved asynchronously (Cao & Carling, 2002)), and (ii) the flow can be

approximated as quasi-steady (i.e., in one-dimensional problems it may be approximated using the backwater equation).

Regarding (i), the decoupling of the equations is acceptable under conditions where the Froude number is smaller than approximately 0.7 (Chavarrías et al., 2019; De Vries, 1965; Lyn, 1987; Lyn & Altinakar, 2002). Such a low Froude value implies that the bed celerity and the celerities associated with the hydrodynamic behavior are of a different order of magnitude and therefore interact only weakly. In rivers with mixed-size sediment, the sorting celerity is assumed to be of a similar order of magnitude as the bed celerity. The sorting celerity is affected by the active layer thickness and may become extremely large for small values of the active layer thickness. However, for physically realistic values of the active layer thickness (for instance, related to the grain size or dune height), the sorting celerity is of a similar order of magnitude as the bed celerity (Ribberink, 1987). Hence, our limitation that the model should be only applied in applications with a Froude number below 0.7 ensures that there is a weak interaction and that the equations may be solved in a decoupled manner.

The main advantage of the proposed method is the fact that it is computationally cheaper than the traditional Monte Carlo method. This has two main reasons. First, the computation of bed level change is typically based on an explicit method in a decoupled solution strategy, where the flow and bed level are updated sequentially. The explicit method implies that the maximum time step is restricted by the Courant-Friedrichs-Lewy (CFL) condition (Courant et al., 1928). For the proposed method, the effective CFL number is a probability density-weighted mean of the mode-specific values of the CFL number. The resulting maximum time step generally is larger than for the traditional Monte Carlo method, which reduces computational time.

Automatic time step selection or a variable time step in the Monte Carlo method may partially eliminate the first advantage. For example, a larger time step could be selected during low flow rates, and a smaller time step during high flow rates. Nevertheless, a limitation for such variable time step selection is the actual duration of a certain flow rate in the hydrograph. A flow rate that has a low probability of occurrence (e.g., only two days in a full year) would automatically be limited to a small time step because of its physical duration even if the stability requirement of the numerical method would enable a time step of several months. In the proposed method, there is no need to limit the time step to a size that is small enough to appreciate changes in the hydrograph and peak flow events to accurately represent the dynamics in a BWS and UBS, and therefore generally a larger time step is allowed.

The second reason for the proposed method to be computationally cheap is related to the smoothness of the solution. The fact that the proposed method does not consider the sequence of short-term variations of the flow, leads to an elimination of small-scale and fast fluctuations of bed level and bed surface texture (e.g., Arkesteijn et al., 2019; Van Vuren et al., 2015). This is attractive from a numerical modeling perspective in that the proposed method provides smoother results than the traditional method, which benefits numerical stability. This indirectly also enables a larger time step in the proposed method in comparison to a single realization in the Monte Carlo analysis.

Although our analysis has addressed one-dimensional models wherein temporal variations in channel width are not considered, we expect that the proposed methodology for treating the boundary conditions can also be applied to one-dimensional models wherein temporal variations in channel width can be parametrically accounted for, or in two-dimensional problems. The static slope-texture approximation is expected to also apply to two-dimensional situations. This, however, should be tested in future research.

7. Conclusions

The time scale of channel response (with respect to channel slope, channel width, and bed surface texture) is usually larger than the one of short-term changes in the controls. This implies that short-term changes of the hydrodynamic controls are not reflected in the channel response. It allows us to assume that, in engineered channels (i.e., fixed-planform channels), channel slope and bed surface texture cannot keep pace with short-term changes of the hydrodynamic controls due to, for instance, the natural variability of the flow rate. This observation has led to the formulation of the "static slope approximation" for the river equilibrium state by Arkesteijn et al. (2019). Here we extend this approximation to the transient phase of channel response. Furthermore, we extend the "static

slope approximation" to the "static slope-texture approximation," as we assume that not only the channel bed slope but also the bed surface texture does not keep pace with short-term changes of the hydrodynamic controls.

We show that, (a) the mean component of the transient channel response (i.e., mean regarding to stochastic controls) is determined by the probability distribution of the controls (e.g., the flow duration curve), while (b) the fluctuating component of channel response depends on the sequence of the control values in a particular realization of the controls. These findings are similar to the effects of the hydrodynamic controls on the quasi-static and dynamic components of the quasi-equilibrium state (Arkesteijn et al., 2019).

The domination of the flow duration curve over the flow rate sequence allow us to develop a rapid numerical method that accounts for the stochastics of the hydrodynamic controls by considering sets of hydrodynamic controls (i.e., modes) and their probability. The model computes the mode-specific flow, (grainsize-specific) sediment transport rates, and bed level change. The net change of bed level and surface texture are then computed by weighting mode-specific values with the probability density of each mode. As a result, the transient channel response predicted by the proposed method is a deterministic one, despite the controls being defined in a stochastic manner.

The proposed method does not explicitly account for the fluctuations on the short time scale, yet is shown to incorporate the mean contribution of these changes well. The proposed method is a two-layer model for mixed-size sediment conservation. In comparison to the traditional Hirano (1972) model, it introduces an additional layer, that is, the dynamic layer, between the active layer and the substrate. The active layer accounts for the sediment that is regularly reworked by the flow, and the dynamic layer represents the bed sediment that is reworked due to alternating aggradation and degradation associated with short-term variation of the controls (i.e., fluctuations that we eliminate). The fluxes between the active layer and dynamic layer directly follow from a mass conservation formulation for this dynamic layer and hence no parametric relations are involved.

The proposed method has been tested successfully against the mean outcome of the traditional Monte Carlo method. The new method is an appropriate and computationally cheap alternative to estimating the mean component of a Monte Carlo analysis, requires less detailed input data, and allows for a significantly larger time step and reduced computation time. Furthermore, these mean results may be obtained within a single model simulation.

The proposed method has been applied to two cases: sea level rise and sediment nourishments. The sea level rise case has shown that sea level rise, despite leading to overall channel bed aggradation, can lead to channel bed erosion downstream of locally wide river reaches.

The method accurately reproduces the typically slow transient channel response to sea level rise, but also for the faster transient channel response to disturbances such as sediment nourishments.

Appendix A: Model Equations

The proposed method as well as the traditional Monte Carlo method, use the same equations for the flow, grainsize-selective transport rates, and change in bed level.

We use the backwater approximation (Chow, 1959) to solve for the quasi-steady flow over a given bed level profile. The backwater equations, for a channel with temporally constant yet spatially variable width, are given by:

$$\frac{\mathrm{d}h}{\mathrm{d}s} = \frac{S - S_f - \mathrm{Fr}^2 \frac{h}{B}\frac{\mathrm{d}B}{\mathrm{d}s}}{1 - \mathrm{Fr}^2}, \quad \forall\ t, \tag{A1}$$

$$\frac{\mathrm{d}Q_w}{\mathrm{d}s} = 0, \quad \forall\ t, \tag{A2}$$

where Q_w [m^3/s] denotes the flow discharge, h the flow depth, s the streamwise coordinate, S [-] is the channel slope ($S = -\partial\eta/\partial x$ where η [m] is the bed level), S_f [-] is the friction slope ($S_f = c_f \mathrm{Fr}^2$), $\mathrm{Fr} = \sqrt{Q_w^2/(gB^2h^3)}$ [-] is the Froude number, B (m) the channel width, and g (m/s^2) is the acceleration due to gravity.

Given the water discharge and flow depth, we compute grainsize-selective transport rates using the sediment transport relation of Ashida and Michiue (1972). This provides us with the grainsize-specific sediment transport capacity of grain size fraction k per unit width, q_{bk0}. Subsequently, this capacity is multiplied by the channel width

B and corrected for the volume fraction content F_{ak} of size fraction k in the bed surface sediment or active layer (with $\sum_{k=1}^{n_f} F_{ak} = 1$ where n_f is the number of grain size fractions) to compute the grainsize-specific sediment transport rate Q_{bk} over the river cross-section:

$$Q_{bk} = BF_{ak}q_{bk0}. \tag{A3}$$

The change in bed level is described using the Exner (1920) equation:

$$B\frac{\partial \eta}{\partial t} = -\frac{1}{1-p}\frac{\mathrm{d}Q_b}{\mathrm{d}s}, \tag{A4}$$

where p [-] is the porosity of the bed sediment and the total sediment load Q_b is given by $Q_b = \sum_{k=1}^{n_f} Q_{bk}$.

Using the traditional Monte Carlo method, the change in bed surface texture is described using the Hirano (1971) equations:

$$B\frac{\partial L_a F_{ak}}{\partial t} = -Bf_k^I\frac{\partial(\eta - L_a)}{\partial t} - \frac{1}{1-p}\frac{\partial Q_{bk}}{\partial s}, \quad \forall k \in (1, n_f - 1). \tag{A5}$$

The sediment in the substrate below is given as:

$$B\frac{\partial L_s f_{sk}}{\partial t} = Bf_k^I\frac{\partial(\eta - L_a)}{\partial t}, \quad \forall k \in (1, n_f - 1). \tag{A6}$$

where f_{sk} [-] denotes the volume fraction content of size fraction k in the top substrate layer having thickness L_s. The layers below are not interacting with the flow and therefore not updated. The volume fraction content of size fraction $k = n_f$ is computed according to the condition $\sum_{k=1}^{n_f} f_{sk} = 1$.

The volume fraction content of size fraction k at the interface between the active layer and the substrate f_k^I is defined as:

$$f_k^I = \begin{cases} f_{sk} & \text{if} \quad \dfrac{\partial(\eta - L_a)}{\partial t} < 0, \\ (1-\alpha)F_{ak} + \alpha\dfrac{Q_{bk}}{Q_b} & \text{if} \quad \dfrac{\partial(\eta - L_a)}{\partial t} > 0, \end{cases} \tag{A7}$$

The grain size distribution of the sediment flux through the interface between the active layer and substrate is equal to the one of the top substrate layer under degradational conditions. Under aggradational conditions, the grain size distribution is equal to a weighted average of the one of the active layer and bed load, with weighting factor α (Hoey & Ferguson, 1994).

The proposed method uses a two-layer model to solve for the change in bed surface texture (Section 2). Sediment in a "dynamic layer" positioned immediately below the active layer is reworked by the flow only occasionally. As such, we assume that its grain size distribution is not important in the computation of the sediment transport rate (Equation A3). The change in bed surface texture is computed as follows:

$$B\frac{\partial L_a F_{ak}}{\partial t} = -Bf_k^I\frac{\partial(\eta - L_a)}{\partial t} - \frac{1}{1-p}\frac{\partial Q_{bk}}{\partial s}, \quad \forall k \in (1, n_f - 1), \tag{A8}$$

$$B\frac{\partial L_d F_{dk}}{\partial t} = Bf_k^I\frac{\partial(\eta - L_a)}{\partial t} - Bf_{dk}^I\frac{\partial(\eta - L_a - L_d)}{\partial t}, \quad \forall k \in (1, n_f - 1), \tag{A9}$$

where F_{dk} the volume fraction content of grain size fraction k in the dynamic layer.

The sediment in the substrate below is given as:

$$B\frac{\partial L_s f_{sk}}{\partial t} = Bf_{dk}^I\frac{\partial(\eta - L_a - L_d)}{\partial t}, \quad \forall k \in (1, n_f - 1). \tag{A10}$$

The grain size distribution of the sediment flux through the interface between the active layer and dynamic layer, f_k^I, is similar to the sediment flux between the active layer and the substrate in the Hirano model. We adopt the Hoey and Ferguson (1994) formulation for the sediment flux and thus allow sediment from the bed load to directly mix into the dynamic layer:

$$f_k^I = \begin{cases} F_{dk} & \text{if} \quad \dfrac{\partial(\eta - L_a)}{\partial t} < 0, \\ (1-\alpha)F_{ak} + \alpha\dfrac{Q_{bk}}{Q_b} & \text{if} \quad \dfrac{\partial(\eta - L_a)}{\partial t} > 0, \end{cases} \tag{A11}$$

The grain size distribution of the sediment flux through the interface between the dynamic layer and the top layer of the substrate, f_{dk}^I, follows from:

$$f_{dk}^I = \begin{cases} f_{sk} & \text{if} \quad \dfrac{\partial(\eta - L_a - L_d)}{\partial t} < 0, \\ F_{dk} & \text{if} \quad \dfrac{\partial(\eta - L_a - L_d)}{\partial t} > 0. \end{cases} \tag{A12}$$

For simplicity, we assume that the active layer thickness, L_a, and the dynamic layer thickness, L_d, are constant in time.

Appendix B: Effect of Dynamic Layer and Its Thickness

This appendix addresses the relevance of the dynamic layer and its thickness. To this end, we compare the proposed method in Figure 2b with a simplified method without dynamic layer in Figure B1.

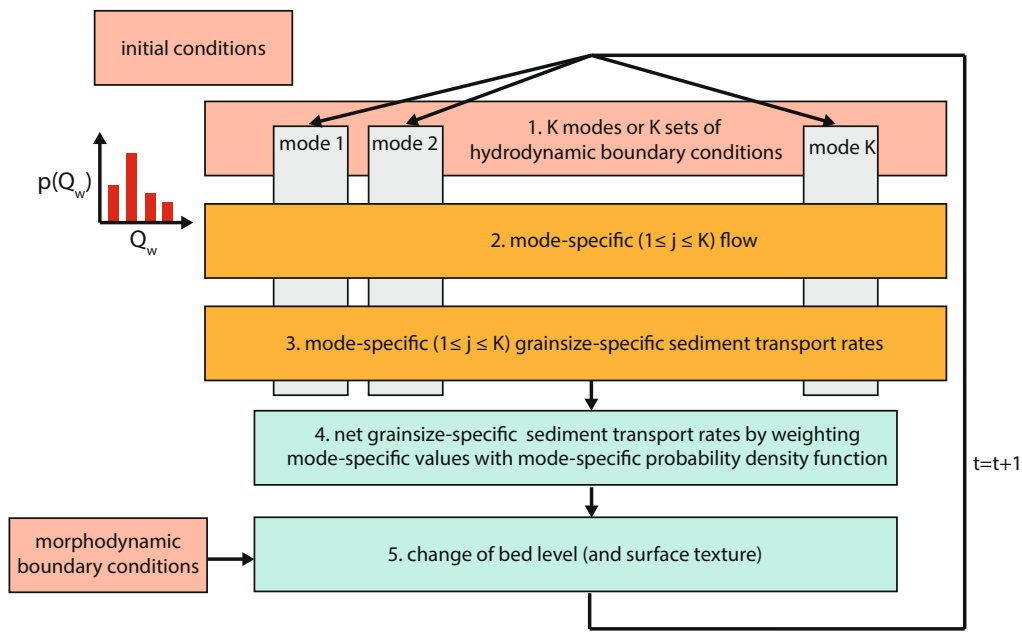

Figure B1. Flow chart of the proposed method under conditions when the dynamic layer can be neglected.

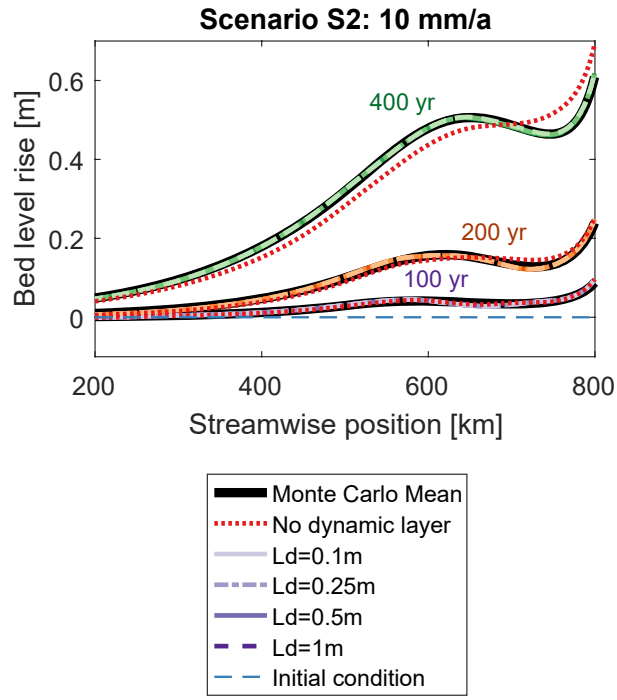

Figure B2. Transient channel response (i.e., change in bed level) to sea level rise scenario S2 using the proposed method for different values of the dynamic layer thickness.

This reduced version of the proposed method neglects the sorting in the substrate just below the active layer. Instead of weighting the mode-specific bed level change, here the net sediment transport rate is computed by weighting the mode-specific sediment transport rates with the mode-specific probability density, and net change in bed level and bed texture are solved based on these net sediment transport rates. This simplified flow chart is computationally cheaper than the method shown in Figure 2b.

The thickness of the dynamic layer is determined by the depth of reworking by the flow. The latter is related to the typical river segments (see Section 3). Significant reworking of the bed by the flow takes place in UBSs and BWSs only. As a result, the dynamic layer is relevant only in these segments. In a QNFS reworking of the bed due to fluctuations in the controls is by definition, insignificant, and as a result, the dynamic layer thickness can be set to zero. Under conditions in which the dynamic layer can be neglected, the flow chart in Figure 2b automatically reduces to the flow chart in Figure B1. This is because the mode-specific grainsize-specific sediment transport rates are approximately the same for all modes, and, as a result, also equal to the average value. The dynamic layer is irrelevant also under unisize sediment conditions.

Figure B2 shows the results of Scenario S2 for runs with varying dynamic layer thickness, and one without a dynamic layer. As shown, the results with a dynamic layer are better than without, yet the value of the active layer thickness does not play a significant role in the considered case. We hypothesize that this is due to the aggradational nature of the case. We recommend further research into the value of the dynamic layer thickness in other cases.

Appendix C: Equilibrium Equations and the Initial Condition

All cases in this paper start from an equilibrium state, which enables us to limit our assessment to the effects of the sea level rise and nourishment specifically. We apply the equilibrium model introduced in Arkesteijn et al. (2019) to find the equilibrium state under a time-varying water discharge (i.e., hydrograph). As Arkesteijn et al. (2019) considered equilibrium under unisize sediment conditions only, we first extend their approach to conditions with mixed-size sediment.

It is important to note that, in a dynamic equilibrium state, the top substrate is reworked by the flow as a result of alternating aggradation and erosion associated with short-term variations of the flow rate. This implies that the top part of the substrate has an equilibrium grain size distribution that is a weighted average of the active layer and annual bed load flux (associated with the Hoey and Ferguson approximation of the vertical sediment flux). This appendix provides the equations describing the grain size distributions of the active layer and the top substrate layer under equilibrium conditions.

If the statistics of the hydrograph, sedigraph, and base level are constant in time, the river reach may tend to a dynamic equilibrium state where the bed level and bed texture vary around stable mean values (Arkesteijn et al., 2019; Blom, Chavarrías, et al., 2017; Lane, 1957; Parker, 2004). This dynamic equilibrium state is characterized by a static component (i.e., the mean or time-averaged longitudinal profile) and a dynamic component (i.e., fluctuation of the bed level and surface texture around a mean state). We start all our runs from the mean, static component of the equilibrium state.

The following equilibrium condition is applied to the bed level, bed surface texture and substrate composition:

$$\lim_{T\to\infty}\frac{1}{T}\int_0^T \frac{\partial \eta(s,t)}{\partial t}\mathrm{d}t = 0. \quad \forall s \tag{C1}$$

$$\lim_{T\to\infty}\frac{1}{T}\int_0^T \frac{\partial F_{ak}(s,t)}{\partial t}\mathrm{d}t = 0. \quad \forall s \tag{C2}$$

$$\lim_{T\to\infty}\frac{1}{T}\int_0^T \frac{\partial f_{sk}(s,t)}{\partial t}\mathrm{d}t = 0. \quad \forall s \tag{C3}$$

These equations state that a reach is in equilibrium when the long term averaged bed level, active layer content and substrate content do not change.

We define the time-averaged mean morphodynamic state, that is, the static component, as:

$$\tilde{\eta} = \lim_{T\to\infty}\frac{1}{T}\int_0^T \eta \ \mathrm{d}t, \quad \forall s \tag{C4}$$

$$\tilde{F}_{ak} = \lim_{T\to\infty}\frac{1}{T}\int_0^T F_{ak} \ \mathrm{d}t, \quad \forall s \tag{C5}$$

$$\tilde{f}_{sk} = \lim_{T\to\infty}\frac{1}{T}\int_0^T f_{sk} \ \mathrm{d}t, \quad \forall s. \tag{C6}$$

and assume that for the computation of the hydrodynamic behavior and the sediment transport rates, the equilibrium state may be approximated by its time-averaged or static state. The latter is the static-slope approximation. For an elaborate discussion on the validity of this approximation, please see Arkesteijn et al. (2019).

The static slope approximation allows us to derive expressions that can be used for the computation of the bed level, the bed surface texture and the substrate texture.

Appendix C1: Bed Level

We start from Equation C1 and substitute the Exner equation (Equation A4):

$$\begin{aligned}\lim_{T\to\infty}\frac{1}{T}\int_0^T \frac{\partial \eta(s,t)}{\partial t}\mathrm{d}t &= -\lim_{T\to\infty}\frac{1}{TB(1-p)}\int_0^T \frac{\partial Q_b}{\partial s}\mathrm{d}t \\ &= -\lim_{T\to\infty}\frac{1}{TB(1-p)}\int_0^T \frac{\partial \sum_{k=1}^{n_f} BF_{ak}\hat{q}_{bk}}{\partial s}\mathrm{d}t = 0\end{aligned}$$

This directly implies that:

$$\lim_{T\to\infty}\int_0^T\left(\sum_{k=1}^{n_f}F_{ak}\hat{q}_{bk}\frac{\partial B}{\partial s}+\sum_{k=1}^{n_f}B\hat{q}_{bk}\frac{\partial F_{ak}}{\partial s}+\sum_{k=1}^{n_f}BF_{ak}\frac{\partial \hat{q}_{bk}}{\partial s}\right)\mathrm{d}t=0 \tag{C7}$$

The above expression contains three spatial derivatives, that is, a derivative of the channel width (which is assumed to be a known function), a derivative of the spatial gradient in bed surface texture, and the derivative of the grain size specific sediment transport capacity. Following the method in Arkesteijn et al. (2019), we use the continuity equation (that is, $Q_w = Buh$) and the backwater equation to express the the latter as a function of the local channel bed slope.

First, we substitute the continuity equation, which yields:

$$\frac{\partial \hat{q}_{bk}}{\partial s}=\frac{\partial \hat{q}_{bk}}{\partial u}\frac{\partial u}{\partial s}=\frac{\partial \hat{q}_{bk}}{\partial u}\left(\frac{1}{Bh}\frac{\partial Q_w}{\partial s}-\frac{Q_w}{B^2h}\frac{\partial B}{\partial s}-\frac{Q_w}{Bh^2}\frac{\partial h}{\partial s}\right)$$

Next, we substitute the backwater equation for the gradient in flow depth:

$$\frac{\partial \hat{q}_{bk}}{\partial s}=\frac{\partial \hat{q}_{bk}}{\partial u}\left(\frac{1}{Bh}\frac{\partial Q_w}{\partial s}-\frac{Q_w}{B^2h}\frac{\partial B}{\partial s}-\frac{Q_w}{Bh^2}\left(\frac{S-S_f-\mathrm{Fr}^2\frac{h}{B}\frac{\mathrm{d}B}{\mathrm{d}s}}{1-\mathrm{Fr}^2}\right)\right) \tag{C8}$$

This expression can be substituted back into Equation C7, leading to:

$$\lim_{T\to\infty}\int_0^T\left(\sum_{k=1}^{n_f}F_{ak}\hat{q}_{bk}\frac{\partial B}{\partial s}+\sum_{k=1}^{n_f}B\hat{q}_{bk}\frac{\partial F_{ak}}{\partial s}+\right.$$

$$\left.\sum_{k=1}^{n_f}BF_{ak}\left(\frac{\partial \hat{q}_{bk}}{\partial u}\left(\frac{1}{Bh}\frac{\partial Q_w}{\partial s}-\frac{Q_w}{B^2h}\frac{\partial B}{\partial s}-\frac{Q_w}{Bh^2}\left(\frac{S-S_f-\mathrm{Fr}^2\frac{h}{B}\frac{\mathrm{d}B}{\mathrm{d}s}}{1-\mathrm{Fr}^2}\right)\right)\right)\right)\mathrm{d}t=0$$

Finally, we apply the static slope approximation and we use the constant multiple rule to bring all constants in front of the integral:

$$\begin{aligned}&\sum_{k=1}^{n_f}F_{ak}\frac{\partial B}{\partial s}\lim_{T\to\infty}\int_0^T\hat{q}_{bk}\mathrm{d}t+\sum_{k=1}^{n_f}B\frac{\partial F_{ak}}{\partial s}\lim_{T\to\infty}\int_0^T\hat{q}_{bk}\mathrm{d}t\\&-S\sum_{k=1}^{n_f}BF_{ak}\lim_{T\to\infty}\frac{1}{T}\int_0^T\frac{\partial \hat{q}_{bk}}{\partial u}\frac{Q_w}{Bh^2}\frac{1}{1-\mathrm{Fr}^2}\mathrm{d}t+\\&\sum_{k=1}^{n_f}BF_{ak}\lim_{T\to\infty}\frac{1}{T}\int_0^T\frac{\partial \hat{q}_{bk}}{\partial u}\left(\frac{1}{Bh}\frac{\partial Q_w}{\partial s}-\frac{Q_w}{B^2h}\frac{\partial B}{\partial s}-\frac{Q_w}{Bh^2}\left(\frac{-S_f-\mathrm{Fr}^2\frac{h}{B}\frac{\mathrm{d}B}{\mathrm{d}s}}{1-\mathrm{Fr}^2}\right)\right)\mathrm{d}t=0\end{aligned} \tag{C9}$$

Equation C9 is an equation with as only unknowns the bed slope and the bed surface texture gradients for the various grain sizes. Given the flow state at a certain river cross section, the channel width and width gradient, and the bed surface texture at that position, all other terms can be calculated.

Under unisize sediment conditions, the above equation significantly simplifies since $F_{a1} = 1$ and $\partial F_{a1}/\partial s = 0$. For the latter case, an explicit expression for the equilibrium channel bed slope can be obtained (Arkesteijn et al., 2019).

Appendix C2: Bed Surface Texture

For the bed surface texture we start from a summation of the Hirano equations for the bed surface texture and the sediment in the substrate below, that is, Equations A5 and A6. Conveniently, the term with the interface flux cancels out. This leads to:

$$B\frac{\partial L_a F_{ak}}{\partial t}+B\frac{\partial L_s f_{sk}}{\partial t}=-\frac{1}{1-p}\frac{\partial Q_{bk}}{\partial s},\quad \forall k\in(1,n_f-1). \tag{C10}$$

Next, we substitute the equilibrium conditions in Equation C2 and C3. This results into:

$$\lim_{T\to\infty}\frac{1}{T}\int_0^T \frac{\partial Q_{bk}(s,t)}{\partial s}\mathrm{d}t = 0.$$

After that, we write the grain size specific sediment transport rate Q_{bk} as the product of the surface texture fraction F_{ak} and the sediment transport capacity if the bed were to consist of a single grainsize only $\hat{Q}_{bk}$. In addition, we expand the derivative using the product rule. This leads to:

$$\lim_{T\to\infty}\frac{1}{T}\int_0^T \frac{\partial F_{ak}\hat{Q}_{bk}(s,t)}{\partial s}\mathrm{d}t = \lim_{T\to\infty}\frac{1}{T}\int_0^T F_{ak}\frac{\partial \hat{Q}_{bk}(s,t)}{\partial s} + \hat{Q}_{bk}\frac{\partial F_{ak}(s,t)}{\partial s}\mathrm{d}t = 0.$$

Next, we apply the static slope approximation and we use the constant multiple rule to bring all constants in front of the integral. This leads to the following expression:

$$F_{ak}\lim_{T\to\infty}\frac{1}{T}\int_0^T \frac{\partial \hat{Q}_{bk}(s,t)}{\partial s}\mathrm{d}t + \frac{\partial F_{ak}(s,t)}{\partial s}\lim_{T\to\infty}\frac{1}{T}\int_0^T \hat{Q}_{bk}\mathrm{d}t = 0,$$

which can be rewritten to:

$$\frac{\partial F_{ak}(s,t)}{\partial s} = -F_{ak}\frac{\lim_{T\to\infty}\frac{1}{T}\int_0^T \frac{\partial \hat{Q}_{bk}(s,t)}{\partial s}\mathrm{d}t}{\lim_{T\to\infty}\frac{1}{T}\int_0^T \hat{Q}_{bk}\mathrm{d}t}\forall k \in (1, n_f - 1). \tag{C11}$$

Please note that, we now have Equation C9 and $n_f - 1$ equations for the bed surface texture gradient. One additional equation for the surface texture gradient further follows from the requirement that the derivative of all fractions together is 0, that is, $\sum_1^{n_f}\partial F_{ak}(s,t)/\partial s = 0$, to maintain that all fractions together sum to one. As a result we have $n_f + 1$ unknown spatial gradients and also $n_f + 1$ equations.

Appendix C3: Numerical Solution

Equation C9, the $n_f - 1$ Equation C11 and the requirement $\sum_1^{n_f}\partial F_{ak}(s,t)/\partial s = 0$ together form a system of first order differential equations. This system has $n_f + 1$ equations, wherein n_f is the number of grain size fractions. The system can be solved numerically, where each of the above integrals is approximated using the probability density function of the water discharge (i.e., the flow duration curve). For a more detailed explanation of how to evaluate such integrals, we refer to Arkesteijn et al. (2019). We solve the equations iteratively to find the bed slope and bed surface texture gradients. Subsequently, the bed level and bed surface texture gradients are used in an explicit numerical scheme to calculate the longitudinal bed profile and bed texture using the space-marching as explained in Arkesteijn et al. (2019).

Appendix C4: Substrate Texture

In addition to the channel bed profile and bed surface texture, we can approximate expressions for the substrate texture (traditional model) or the dynamic layer texture (proposed model). Below, we illustrate the derivation for the traditional model. The derivation for the proposed model and the dynamic layer texture, however, is analogous.

We start from Equation C3; and substitute the substrate equation and the Hoey-Ferguson flux formulation:

$$\begin{aligned}\lim_{T\to\infty}\frac{1}{T}\int_0^T f_{kI}\frac{\partial\eta}{\partial t}\mathrm{d}t &= \lim_{T\to\infty}\frac{1}{T}\int_0^T f_{kI}\frac{\partial\eta}{\partial t}1_{\frac{\partial\eta}{\partial t}>0}\mathrm{d}t + \lim_{T\to\infty}\frac{1}{T}\int_0^T f_{kI}\frac{\partial\eta}{\partial t}1_{\frac{\partial\eta}{\partial t}<0}\mathrm{d}t \\ &= \lim_{T\to\infty}\frac{1}{T}\int_0^T \left((1-\alpha)F_{ak} + \alpha\frac{Q_{bk}}{Q_b}\frac{\partial\eta}{\partial t}\right)1_{\frac{\partial\eta}{\partial t}>0}\mathrm{d}t \\ &\quad + \lim_{T\to\infty}\frac{1}{T}\int_0^T f_{sk}\frac{\partial\eta}{\partial t}1_{\frac{\partial\eta}{\partial t}<0}\mathrm{d}t = 0\end{aligned} \tag{C12}$$

Next, we apply the static slope approximation and we use the constant multiple rule to bring all constants in front of the integral:

$$(1-\alpha)F_{ak}\lim_{T\to\infty}\frac{1}{T}\int_0^T\frac{\partial\eta}{\partial t}1_{\frac{\partial\eta}{\partial t}>0}\mathrm{d}t+\lim_{T\to\infty}\frac{1}{T}\int_0^T\alpha\frac{Q_{bk}}{Q_b}\frac{\partial\eta}{\partial t}1_{\frac{\partial\eta}{\partial t}>0}\mathrm{d}t+$$

$$f_{sk}\lim_{T\to\infty}\frac{1}{T}\int_0^T\frac{\partial\eta}{\partial t}1_{\frac{\partial\eta}{\partial t}<0}\mathrm{d}t=0$$

These equations may be simplified by using the following equilibrium condition on the bed level, that is, the average of all erosion in equilibrium equals the average of all deposition in equilibrium:

$$\lim_{T\to\infty}\frac{1}{T}\int_0^T\frac{\partial\eta}{\partial t}1_{\frac{\partial\eta}{\partial t}>0}\mathrm{d}t+\lim_{T\to\infty}\frac{1}{T}\int_0^T\frac{\partial\eta}{\partial t}1_{\frac{\partial\eta}{\partial t}<0}\mathrm{d}t=0$$

We may use this equilibrium property to further simplify the above equation and obtain:

$$((1-\alpha)F_{ak}-f_{sk})\lim_{T\to\infty}\frac{1}{T}\int_0^T\frac{\partial\eta}{\partial t}1_{\frac{\partial\eta}{\partial t}>0}\mathrm{d}t+\alpha\lim_{T\to\infty}\frac{1}{T}\int_0^T\frac{Q_{bk}}{Q_b}\frac{\partial\eta}{\partial t}1_{\frac{\partial\eta}{\partial t}>0}\mathrm{d}t=0$$

We now find the following expression for the substrate texture. Please note that, this expression only relates to the substrate that actively interferes with the flow in equilibrium conditions whereas an expression for the deeper substrate layers cannot be defined using the following equation:

$$f_{sk}=(1-\alpha)F_{ak}+\alpha\frac{\lim_{T\to\infty}\frac{1}{T}\int_0^T\frac{Q_{bk}}{Q_b}\frac{\partial\eta}{\partial t}1_{\frac{\partial\eta}{\partial t}>0}\mathrm{d}t}{\lim_{T\to\infty}\frac{1}{T}\int_0^T\frac{\partial\eta}{\partial t}1_{\frac{\partial\eta}{\partial t}>0}\mathrm{d}t}=0 \tag{C13}$$

Equation C13 illustrates how the parameter α affects the substrate texture in the equilibrium state. Channel bed aggradation leads to a sediment flux from the active layer to the top substrate layer. When selecting $\alpha=0$, this sediment flux has the same grain size distribution as the active layer, and not surprisingly, the texture in the substrate is found to be the same as in the active layer, that is, $f_{sk}=F_{ak}$. On the contrary, when $\alpha\neq0$, part of the bed load mixes into the substrate and a different equilibrium grain size is found in the top substrate layer.

To derive the composition of the dynamic layer, the same procedure as above can be followed, wherein we start from the following equation instead of Equation C12:

$$\lim_{T\to\infty}\frac{1}{T}\int_0^T\left(f_{dk}^I-f_k^I\right)\frac{\partial\eta}{\partial t}\mathrm{d}t=0 \tag{C14}$$

Substitution of the respective interface fluxes leads to a similar expression as derived above for the top substrate layer of the traditional model in Equation C13 above. More precisely, the derivation provides the following result:

$$2F_{dk}-f_{sk}=F_{dk}=(1-\alpha)F_{ak}+\alpha\frac{\lim_{T\to\infty}\frac{1}{T}\int_0^T\frac{Q_{bk}}{Q_b}\frac{\partial\eta}{\partial t}1_{\frac{\partial\eta}{\partial t}>0}\mathrm{d}t}{\lim_{T\to\infty}\frac{1}{T}\int_0^T\frac{\partial\eta}{\partial t}1_{\frac{\partial\eta}{\partial t}>0}\mathrm{d}t}=0 \tag{C15}$$

Here, it should be noted that the first equality holds because $F_{dk}=f_{sk}$. This is because for the proposed model, channel bed aggradation leads to a sediment flux from the dynamic layer to the top substrate layer. This sediment flux has the same grain size distribution as the dynamic layer and the reverse holds under degradational conditions. Consequently the layers have the same composition. The mathematical derivation for this equality is the same as for the top substrate layer in the traditional model with $\alpha=0$ above.

Appendix D: Number of Modes of the Controls

The proposed method is based on K sets of boundary conditions or modes. A total number of 36,500 daily discharges are present in our water discharge record at Lobith between 1901 and 2000 (for the sake of simplicity we have removed the additional day of leap years). These values are recorded as rounded integers, and therefore only

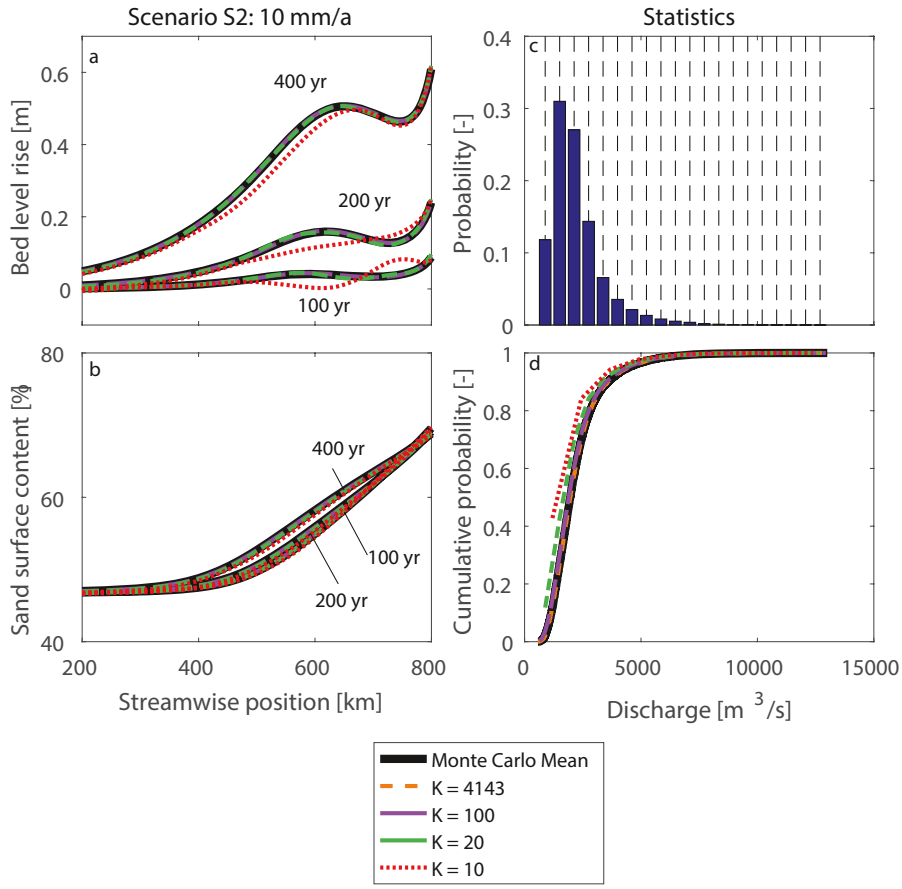

Figure D1. Transient channel response to sea level rise scenario S2. Panels (a) and (b) show the change in bed level and surface sand content, Panel (c) shows the probability of each bin for $K = 20$ modes, and panel (d) shows the cumulative probability densities for different values of the number of modes.

a total number of 4,143 unique daily discharge values are present. Hence, selecting $K = 4{,}143$ modes would lead to the same flow duration curve as the flow duration curve associated with the hydrograph imposed in the Monte Carlo method. As such, we consider $K = 4{,}143$ to provide the most accurate approximation in terms of discretizing our probability density function, as a smaller number of modes could lead to a reduced accuracy because of discretization errors. This appendix compares the outcome for $K = 4{,}143$ with smaller values for the number of modes K and motivates our choice for $K = 20$.

We determine the K modes or bins linearly between the lowest (500 m^3/s) and highest water discharge (13,000 m^3/s) within the 100-year hydrograph record. The frequency of discharges in each of these bins has been assigned to the mean (center) value of the bin. Figure D1c shows an example for $K = 20$.

Figures D1a and D1b shows the transient channel response to scenario S2 for different values of the number of modes. Adopting 10 modes introduces a discretization error, and for $K = 20$ and larger values, the results do not vary, which illustrates that it suffices here to discretize the hydrograph into 20 modes.

The number of modes has a large effect on the computation time. Table D1 shows the required computation time for a realization of the Monte Carlo in comparison to the required computation time for a different number of modes K. For a Monte Carlo approximation, N simulations need to be carried out. We have selected $N = 100$ in our cases but a smaller number likely also suffices, for example, $N = 40$ (Van Vuren, 2005).

Table D1
Computation Times for Case 1 (Scenario S2). The Proposed Method Adopts a Time Step of Half a Month (1/24 of a Year), Which is Approximately 15.2 Days

	1 Monte Carlo realization	Monte Carlo	$K = 4{,}143$	$K = 100$	$K = 20$	$K = 10$
Δt	1 day	–	15.2 days	15.2 days	15.2 days	15.2 days
Duration	17 min	$N \times 17$ min	34 hr22 min	42 min	10 min	6 min

Data Availability Statement

The model is available at https://zenodo.org/record/5778956. All data for this paper are cited and referred to in the reference list.

Acknowledgments
This research is part of the research programme RiverCare, supported by the Dutch Technology Foundation TTW, which is part of the Netherlands Organization for Scientific Research (NWO), and which is partly funded by the Ministry of Economic Affairs under grant number P12-14 (Perspective Programme). We thank the Editor Mikael Attal, the Associate Editor, Chenge An, Zheng Bing Wang, and an anonymous reviewer for their helpful comments on the manuscript.

References

An, C., Cui, Y., Fu, X., & Parker, G. (2017). Gravel-bed river evolution in earthquake-prone regions subject to cycled hydrographs and repeated sediment pulses. *Earth Surface Processes and Landforms*, *42*(14), 2426–2438. https://doi.org/10.1002/esp.4195

An, C., Fu, X., Wang, G., & Parker, G. (2017). Effect of grain sorting on gravel bed river evolution subject to cycled hydrographs: Bed load sheets and breakdown of the hydrograph boundary layer. *Journal of Geophysical Research: Earth Surface*, *122*(8), 1513–1533. https://doi.org/10.1002/2016JF003994

Arkesteijn, L., Blom, A., Czapiga, M. J., Chavarrías, V., & Labeur, R. J. (2019). The quasi-equilibrium longitudinal profile in backwater reaches of the engineered alluvial river: A space-marching method. *Journal of Geophysical Research: Earth Surface*, *124*(11), 2542–2560. https://doi.org/10.1029/2019JF005195

Ashida, K., & Michiue, M. (1971). An investigation of river bed degradation downstream of a dam. *Proceedings of IAHR, 14th Congress*, *3*, 247–255.

Ashida, K., & Michiue, M. (1972). Study on hydraulic resistance and bed-load transport rate in alluvial streams. *Japan Society of Civil Engineers*, *206*, 59–69. https://doi.org/10.2208/jscej1969.1972.206_59

Blom, A. (2008). Different approaches to handling vertical and streamwise sorting in modeling river morphodynamics. *Water Resources Research*, *44*(3), W03415. https://doi.org/10.1029/2006WR005474

Blom, A., Arkesteijn, L., Chavarrías, V., & Viparelli, E. (2017). The equilibrium alluvial river under variable flow, and its channel-forming discharge. *Journal of Geophysical Research: Earth Surface*, *122*, 1924–1948. https://doi.org/10.1002/2017JF004213

Blom, A., Chavarrías, V., Ferguson, R. I., & Viparelli, E. (2017). Advance, retreat, and halt of abrupt gravel-sand transitions in alluvial rivers. *Geophysical Research Letters*, *44*, 1–10. https://doi.org/10.1002/2017GL074231

Blom, A., & Parker, G. (2004). Vertical sorting and the morphodynamics of bed-form dominated rivers: A modeling framework. *Journal of Geophysical Research*, *109*, F02007. https://doi.org/10.1029/2003JF000069

Blom, A., Viparelli, E., & Chavarrías, V. (2016). The graded alluvial river: Profile concavity and downstream fining. *Geophysical Research Letters*, *43*, 1–9. https://doi.org/10.1002/2016GL068898

Bolla Pittaluga, M., Tambroni, N., Canestrelli, A., Slingerland, R., Lanzoni, S., & Seminara, G. (2015). Where river and tide meet: The morphodynamic equilibrium of alluvial estuaries. *Journal of Geophysical Research: Earth Surface*, *120*(1), 75–94. https://doi.org/10.1002/2014JF003233

Cao, Z., & Carling, P. A. (2002). Mathematical modelling of alluvial rivers: Reality and myth. Part 1: General review. *Proceedings of the Institution of Civil Engineers Water & Maritime Engineering*, *154*(3), 207–219. https://doi.org/10.1680/wame.2002.154.3.207

Chatanantavet, P., & Lamb, M. P. (2014). Sediment transport and topographic evolution of a coupled river and river plume system: An experimental and numerical study. *Journal of Geophysical Research: Earth Surface*, *119*(6), 1263–1282. https://doi.org/10.1002/2013JF002810

Chavarrías, V., Arkesteijn, L., & Blom, A. (2019). A well-posed alternative to the Hirano active layer model for rivers with mixed-size sediment. *Journal of Geophysical Research: Earth Surface*, *124*(11), 2491–2520. https://doi.org/10.1029/2019JF005081

Chow, V. T. (1959). In H. E. Davis (Ed.), *Open-channel hydraulics*. McGraw-Hill.

Courant, R., Friedrichs, K., & Lewy, H. (1928). Über die partiellen differenzengleichungen der mathematischen physik. *Mathematische Annalen*, *100*, 32–74. https://doi.org/10.1007/bf01448839

De Vriend, H. (2015). The long-term response of rivers to engineering works and climate change. *Proceedings – Institution of Civil Engineers*, *168*(CE3), 139–144. https://doi.org/10.1680/cien.14.00068

De Vries, M. (1965). *Considerations about non-steady bed load transport in open channels* (Technical Report No. 36). Delft Hydraulics Laboratory.

De Vries, M. (1975). A morphological time-scale for rivers. In *Proceedings of the XVIth IAHR congress*.

Exner, F. M. (1920). Zur Physik der Dünen. *Akad. Wiss. Wien Math. Naturwiss*, *129*(2a), 929–952 (in German).

Ganti, V., Chadwick, A. J., Hassenruck-Gudipati, H. J., Fuller, B. M., & Lamb, M. P. (2016). Experimental river delta size set by multiple floods and backwater hydrodynamics. *Science Advances*, *2*(5). https://doi.org/10.1126/sciadv.1501768

Hirano, M. (1971). River bed degradation with armoring. *Proceedings of the Japan Society of Civil Engineer*, *195*, 55–65. https://doi.org/10.2208/jscej1969.1971.195_55

Hirano, M. (1972). Studies on variation and equilibrium state of a river bed composed of nonuniform material. *Proceedings of the Japan Society of Civil Engineer*, *207*, 128–129. https://doi.org/10.2208/jscej1969.1972.207_51

Hoey, T. B., & Ferguson, R. (1994). Numerical simulation of downstream fining by selective transport in gravel bed rivers: Model development and illustration. *Water Resources Research*, *30*(7), 2251–2260. https://doi.org/10.1029/94WR00556

Howard, A. D. (1982). Equilibrium and time scales in geomorphology: Application to sand-bed alluvial streams. *Earth Surface Processes and Landforms*, *7*(4), 303–325. https://doi.org/10.1002/esp.3290070403

Huthoff, F., van Vuren, S., Barneveld, H., & Scheel, F. (2010). On the importance of discharge variability in the morphodynamic modeling of rivers. In *Proc. Int. Conf. On fluvial hydraulics* (pp. 985–991)

Klein Tank, A., Beersma, J., Bessembinder, J., Hurk, B. V. D., & Lenderink, G. (2015). *KNMI'14 klimaatscenario's voor Nederland* (Technical Report No. 1220042-004). KNMI.

Klijn, F., Hegnauer, M., Beersma, J., & Sperna Weiland, F. (2015). *Wat betekenen de nieuwe klimaatscenario's voor de rivierafvoeren van Rijn en Maas?* (Technical Report No. 1220042-004). Deltares/KNMI.

Lamb, M. P., Nittrouer, J. A., Mohrig, D., & Shaw, J. (2012). Backwater and river plume controls on scour upstream of river mouths: Implications for fluvio-deltaic morphodynamics. *Journal of Geophysical Research*, *117*. https://doi.org/10.1029/2011JF002079

Lane, E. W. (1957). *A study of the shape of channels formed by natural streams flowing in erodible material*. US Army Engineer Division, Missouri River Corps of Engineers.

Lyn, D. (1987). Unsteady sediment transport modeling. *Journal of Hydraulic Engineering*, *113*(1), 1–15. https://doi.org/10.1061/(ASCE)0733-9429(1987)113:1(1)

Lyn, D., & Altinakar, M. (2002). St. Venant-Exner equations for near-critical and transcritical flows. *Journal of Hydraulic Engineering*, *128*(6), 579–587. https://doi.org/10.1061/(ASCE)0733-9429(2002)128:6(579)

Mackin, J. H. (1948). Concept of the graded river. *The Geological Society of America Bulletin*, *59*(5), 463–512. https://doi.org/10.1130/0016-7606(1948)59[463:cotgr]2.0.co;2

Meirovich, L., Laronne, J. B., & Reid, I. (1998). The variation of water-surface slope and its significance for bedload transport during floods in gravel-bed streams. *Journal of Hydraulic Research*, *36*(2), 147–157. https://doi.org/10.1080/00221689809498630

Nittrouer, J. A., Mohrig, D., Allison, M. A., & Peyret, A.-P. B. (2011). The lowermost Mississippi River: A mixed bedrock-alluvial channel. *Sedimentology*, *58*(7), 1914–1934. https://doi.org/10.1111/j.1365-3091.2011.01245.x

Nittrouer, J. A., Shaw, J., Lamb, M. P., & Mohrig, D. (2012). Spatial and temporal trends for water-flow velocity and bed-material sediment transport in the lower Mississippi River. *The Geological Society of America Bulletin*, *124*(3–4), 400–414. https://doi.org/10.1130/B30497.1

Paola, C., & Leeder, M. (2011). Environmental dynamics: Simplicity versus complexity. *Nature*, *469*, 38–39. https://doi.org/10.1038/469038a

Paola, C., & Voller, V. R. (2005). A generalized Exner equation for sediment mass balance. *Journal of Geophysical Research*, *110*, F04014. https://doi.org/10.1029/2004JF000274

Parker, G. (2004). Response of the gravel bed of a mountain river to a hydrograph. In *Proceedings of International Conference on Slopeland disaster mitigation*.

Parker, G., Hassan, M., & Wilcock, P. (2008). Adjustment of the bed surface size distribution of gravel-bed rivers in response to cycled hydrograph. In H. P. H. Habersack & M. Rinaldi (Eds.), *Gravel-bed rivers VI: From process understanding to river restoration* (pp. 241–285). https://doi.org/10.1016/S0928-2025(07)11127-5

Phillips, B. C., & Sutherland, A. J. (1989). Spatial lag effects in bed load sediment transport. *Journal of Hydraulic Research*, *27*(1), 115–133. https://doi.org/10.1080/00221688909499247

Quick, I., König, F., Baulig, Y., Schriever, S., & Vollmer, S. (2020). Evaluation of depth erosion as a major issue along regulated rivers using the classification tool valmorph for the case study of the lower rhine. *International Journal of River Basin Management*, *18*(2), 191–206. https://doi.org/10.1080/15715124.2019.1672699

Ribberink, J. S. (1987). *Mathematical modelling of one-dimensional morphological changes in rivers with non-uniform sediment* (Doctoral Dissertation). Delft University of Technology.

Roelvink, J. (2006). Coastal morphodynamic evolution techniques. *Coastal Engineering*, *53*, 277–287. https://doi.org/10.1016/j.coastaleng.2005.10.015

Saint-Venant, A. J. C. B. (1871). Théorie du mouvement non permanent des eaux, avec application aux crues des rivières et à l'introduction des marées dans leur lit. *Comptes Rendus des séances de l'Académie des Sciences*, *73*, 237–240.

Van Vuren, S. (2005). *Stochastic modelling of river morphodynamics* (Doctoral Dissertation). Delft University of Technology.

Van Vuren, S., de Vriend, H., & Barneveld, H. (2016). A stochastic model approach for optimisation of lowland river restoration works. *Journal of Earth Sciences*, *27*(1), 55–67. https://doi.org/10.1007/s12583-016-0629-0

Van Vuren, S., Paarlberg, A., & Havinga, H. (2015). The aftermath of room for the river and restoration works: Coping with excessive maintenance dredging. *Journal of Hydro-Environment Research*, *9*(2), 172–186. https://doi.org/10.1016/j.jher.2015.02.001

Viparelli, E., Blom, A., & Parker, G. (2012). Modeling stratigraphy formed by prograding Gilbert-type deltas. In *River flow 2012: Proceedings of the international conference on fluvial hydraulics* (pp. 5–7).

Wilmink, R. (2015). *Accelerated morphological modelling* (Master Thesis). University of Twente.

Wong, M., & Parker, G. (2006). One-dimensional modeling of bed evolution in a gravel bed river subject to a cycled flood hydrograph. *Journal of Geophysical Research*, *111*(F3), F03018. https://doi.org/10.1029/2006JF000478

Ylla Arbós, C., Blom, A., Viparelli, E., Reneerkens, M., Frings, R., & Schielen, R. (2021). River response to anthropogenic modification: Channel steepening and gravel front fading in an incising river. *Geophysical Research Letters*, *48*(4), e2020GL091338. https://doi.org/10.1029/2020GL091338